nature communications

Article

https://doi.org/10.1038/s41467-024-52252-2

TCF-1 and TOX regulate the memory formation of intestinal group 2 innate lymphoid cells in asthma

Received: 18 December 2023

Accepted: 31 August 2024

Published online: 08 September 2024

Check for updates

Kaifan Bao[1,2] ✉, Xiaoqun Gu[1], Yajun Song[1], Yijing Zhou[1], Yanyan Chen[1], Xi Yu[3], Weiyuan Yuan[1], Liyun Shi[2], Jie Zheng[1,4] ✉ & Min Hong[1] ✉

Immune memory has been expanded to group 2 innate lymphoid cells (ILC2s), but the cellular and molecular bases remain incompletely understood. Based on house dust mite (HDM)-induced mice asthma models and human samples, we applied flow cytometry, parabiosis, in vivo imaging and adoptive transplantation to confirm the persistence, migration and function of $CD45^+lineage^-CD90.2^+NK1.1^-NKp46^-ST2^-KLRG1^+IL\text{-}17RB^+$ memory-like ILC2s (ml-ILC2s). Regulated by CCR9/CCL25 and S1P signaling, ml-ILC2s reside in the lamina propria of small intestines (siLP) in asthma remission, and subsequently move to airway upon re-encountering antigens or alarmins. Furthermore, ml-ILC2s possess properties of longevity, potential of rapid proliferation and producing IL-13, and display transcriptional characteristics with up-regulation of *Tox* and *Tcf-7*. ml-ILC2s transplantation restore the asthmatic changes abrogated by *Tox* and *Tcf7* knockdown. Our data identify siLP ml-ILC2s as a memory-like subset, which promotes asthma relapse. Targeting TCF-1 and TOX might be promising for preventing asthma recurrence.

Asthma is a chronic airway disorder dominated by type 2 immune responses, which affected nearly 358 million populations globally in 2015 as reported[1]. In developing countries like China, changes in environment and lifestyle during modernization might have given rapid rise to the incidence of asthma from 1.24% to 4.2% in the last two decades[2]. Although the prevalence is still lower than the estimates in developed countries like the UK[3,4], the growing rate of asthma and the shortcomings of existing medications, such as inevitable adverse effects along with long-term application for seizure control[5–7], urge us to better understand the pathogenesis of this refractory airway disease and develop novel therapeutic strategies to treat asthma.

After repeated allergen exposure, antigen-specific T helper 2 (Th2) cells have been well-recognized as the principal source of the type 2 cytokines interleukin (IL)−4, IL-5 and IL-13, contributing to the pathophysiological features of allergic asthma. In recent years, more and more studies have shown that group 2 innate lymphoid cells (ILC2s) resemble Th2 cells in producing type 2 cytokines and mediating allergic inflammation[8,9]. In contrast with Th2 cells, ILC2s are antigen non-specific and could be directly activated by alarmins like IL-33, IL-25 and thymic stromal lymphopoietin (TSLP) released by epithelial cells upon stress or allergen exposure[10]. Classically, partially activated $CD4^+$ Th2 cells will differentiate into memory subsets, which possess the capability to migrate in vivo and respond rapidly upon another contact of the same allergen, mediating inflammatory responses. Interestingly, the immunological memory has been extended to innate immune cells as evidenced by recent studies[11–13]. IL-33 or papain-experienced ILC2s persist in lungs drain lymph nodes (LNs), and respond rapidly to another allergen exposure, which display memory-like characteristics[14]. Moreover, a subset of IL-10-producing ILC2s, termed $ILC2_{10}$, contracted after stimulus removal and persisted in vivo

[1]Jiangsu Key Laboratory for Pharmacology and Safety Evaluation of Chinese Materia Medica, School of Pharmacy, Nanjing University of Chinese Medicine, Nanjing 210023, China. [2]Department of Immunology, School of Medicine, Nanjing University of Chinese Medicine, Nanjing 210023, China. [3]Nanjing Haikerui Pharmaceutical Technology Co., LTD, Nanjing 210023, China. [4]Department of Pharmacology, School of Medicine, Nanjing University of Chinese Medicine, Nanjing 210023, China. ✉e-mail: bkf0824@njucm.edu.cn; jessiezheng@njucm.edu.cn; minhong@njucm.edu.cn

to respond positively to minimal IL-33 stimulation[15]. After multiple exposures to the *Alternaria* allergen extract, lung ICOS$^+$ST2$^+$ILC2s acquire memory, enabling them to elicit asthma-like responses[16]. These incidences suggested that ILC2s might acquire memory characteristics like persistence and quick response. Despite these advances, whether memory ILC2s possess in vivo migrating capability as observed in memory T cells has yet to be investigated, and more in-depth studies are needed to define the memory phenotype of ILC2s in allergic immune responses.

Killer-cell lectin-like receptor G1 (KLRG1), expressed by mature natural killer (NK) cells, CD4$^+$ and CD8$^+$αβ T cells, has been used as a marker to discriminate short-lived effector cells from long-lived memory cell precursors[17]. KLRG1 is found expressed on certain subsets of ILC2s[18–20]. Generally, KLRG1 is considered a co-inhibitory receptor of ILC2s, and the activation of it by its ligand, E-cadherin, has been shown to inhibit effector response of ILC2s[21]. However, recent studies have demonstrated that a group of KLRG1^{hi} inflammatory ILC2s (iILC2s) are potent to expulse invaded *Nippostrongylus brasiliensis* (*N. brasiliensis*)[20,22]. Thus, the role of KLRG1 in regulating ILC2s remains controversial. In addition, KLRG1$^+$ILC2s were reported as intestinal ILC2s[23] and acquire migrating property, which enables them to traffic from intestine to lungs in *N. brasiliensis* infection[20]. Despite the fact that intestine invasion is one of the characteristics of this hookworm infection, certain ILC2s subsets are migratory and are speculated to contribute to various host defense responses.

In this present study based on house-dust-mite (HDM)-induced mice models and clinical asthmatic participants, we find that the long-living ST2$^-$KLRG1$^+$IL-17RB$^+$ ml-ILC2 subset retains strong capability of proliferation and expansion, and producing type 2 cytokines like IL-13 in vivo and in vitro. Mice ml-ILC2s reside in the lamina propria of small intestine (siLP) in remission, and move to airway to induce inflammatory responses upon re-exposure to allergen or alarmins. Furthermore, high levels of genes related with memory T (T_{mem}) cell formation and function like *thymocyte selection-associated high mobility group box (Tox)*, *transcription factor 7, T cell-specific (Tcf7)* and *Il7r*, etc., are identified in both mice and human ml-ILC2s, indicating that ST2$^-$KLRG1$^+$IL-17RB$^+$ ILC2s possess similar transcriptional characteristics with $T_{mem.}$ *Tcf7* and *Tox* knockdown abrogated the memory-like properties of ml-ILC2s, indicating that these transcriptional factors are essential in ml-ILC2s development.

Results

Mice ST2$^-$KLRG1$^+$IL-17RB$^+$ ILC2s with IL-13-producing potentialities accumulate in siLP in asthma remission

To assess the kinetics of different ILC2 subsets during the asthma process, we established an i.p. HDM sensitization model and collected samples at various time points (Fig. 1A). As a result, airway hyperresponsiveness (AHR), elevated serum IgE, eosinophils in peripheral blood, protein levels of type 2 cytokines in lung homogenates and varied cytology in bronchoalveolar lavage fluid (BALF) all restored to the levels of the control group 7 days after challenge (D30), which is physiologically relevant to the steady state of asthma (Fig. 1B–F). Furthermore, flow cytometry analysis showed difference of type 2 immune cells kinetics (Fig. 1G, H, Fig. S1). Specifically, CD4$^+$GATA3$^+$ Th2s increased in PBMC, mediastinal LN and lungs during asthma exacerbation on day 24 (Fig. S1A). As shown in Fig. S1B–D, ST2$^-$KLRG1$^+$IL-17RB$^+$ ILC2s markedly raised in PBMC, mediastinal LN and lungs upon asthma attack, whereas ST2$^-$KLRG1$^+$IL-17RB$^-$ ILC2s showed negligible changes numerically. In addition, ST2$^+$ ILC2s only rose in lungs, which is consistent with the previous report that ST2$^+$ ILC2s are a tissue-resident subset while KLRG1$^+$ ILC2s are a circulating population[20]. Most notably, ST2$^-$KLRG1$^+$IL-17RB$^+$ ILC2s were abundant in siLP rather than other sites at remission phase, in sharp contrast with Th2s and other ILC2s subsets, including ST2$^+$ and ST2$^-$KLRG1$^+$IL-17RB$^-$ (Fig. 1H, Fig. S1A–D). Since intraperitoneal injection of HDM applied in the i.p. HDM sensitization model may induce systemic immune activation, we established another 12-day asthmatic mice model with only airway exposure of HDM (Fig. S2A–F). Similarly, increased frequency and number of ST2$^-$KLRG1$^+$IL-17RB$^+$ ILC2s were found in siLP on day 19 while other asthmatic changes restored (remission phase) (Fig. S2G).

We next sought to give a more detailed picture on type 2 cytokine-producing potential of the ST2$^-$KLRG1$^+$IL-17RB$^+$ ILC2 subset during asthma remission (Fig. 1I–L, Fig. S1E–G, Fig. S2H–K). The proportion and mean fluorescence intensity (MFI) analysis suggested that ST2$^-$KLRG1$^+$IL-17RB$^+$ ILC2s in siLP retained great potentialities for producing IL-13 instead of IL-5 (Fig. 1I, J). In addition, we found that ST2$^-$KLRG1$^+$IL-17RB$^+$ ILC2s were the primary potential source of IL-13 while IL-5 was more likely from Th2s (Fig. 1K, L). IL-4, in contrast, was not detected from ST2$^-$KLRG1$^+$IL-17RB$^+$ ILC2s, and Th2s, ST2$^+$ILC2s, and other cells like mast cells, basophils and eosinophils are the main source of elevated IL-4 in lungs (Fig. S1G). Similar results were determined in the 12-day asthmatic mice model as well (Fig. S2H–K). These data indicated that the ST2$^-$KLRG1$^+$IL-17RB$^+$ ILC2 subset accumulated in siLP and possessed strong IL-13-producing capability in remission of HDM-induced asthma.

In addition, as alarmins IL-25, IL-33, and TSLP are the pro-inflammatory factors activating ILC2s, we assessed the contribution of these cytokines inducing ST2$^-$KLRG1$^+$IL-17RB$^+$ ILC2s both in lungs and siLP at different phases (Fig. S3A). As a result, ST2$^-$KLRG1$^+$IL-17RB$^+$ ILC2s markedly increased in lungs after intranasal IL-25 stimulation (Fig. S3B), and accumulated in siLP 12 days later (Fig. S3C). Of note, the combination of IL-25 and IL-33 further induced this subset of ILC2s while IL-33 or TSLP alone showed negligible effect. These data suggested IL-25 played a pivotal role in inducing ST2$^-$KLRG1$^+$IL-17RB$^+$ ILC2s, and IL-33 might serve as a synergistic role. Interestingly, the combination of IL-25 and TSLP did not show similar efficacy as observed in IL-25 + IL-33. Sam et al. [24]. report that IL-33 signals via a ST2-independent pathway. Instead, IL-33 binds to receptor for advanced glycation end products (RAGE) to signal via epidermal growth factor receptor (EGFR), which subsequently induces mucin hypersecretion and alters the differentiation of airway epithelial cells. This might help to explain the synergistic efficacy of IL-33 stimulating ST2-negative ml-ILC2s. Thus, airway stimulation with alarmins, especially IL-25, can induce the accumulation of ST2$^-$KLRG1$^+$IL-17RB$^+$ ILC2s in siLP, inconsistent with HDM.

Hence, we found that ST2−KLRG1+IL-17RB+ ILC2s accumulated in siLP and retained type 2 cytokine IL-13-producing potential when allergen or non-allergen-induced- airway inflammatory responses emerged, raising the possibility that siLP serves as a reservoir of asthma relapse-promoting ST2$^-$KLRG1$^+$IL-17RB$^+$ ILC2s.

Adoptive transfer of ST2$^-$KLRG1$^+$IL-17RB$^+$ ILC2s from siLP is able to induce asthmatic attack

As shown in Fig. S4, analysis of dynamic changes during different time points of asthma relapse suggested that siLP ST2$^-$KLRG1$^+$IL-17RB$^+$ ILC2s aggregated in remission and then decreased upon another allergen exposure. Meanwhile, this specific subset of ILC2s significantly increased in lungs upon asthma attack coincidentally. We then attempted to determine if ST2$^-$KLRG1$^+$IL-17RB$^+$ ILC2s identified in siLP were the source of these cells in lungs driving asthma relapse. For this, CD45.1$^+$lineage$^-$CD90.2$^+$NK1.1$^-$NKp46$^-$GATA3$^+$ST2$^-$KLRG1$^+$IL-17RB$^+$ ILC2s were sorted from in vitro culturing lineage-negative cells derived from bone marrow (BM), spleen, lungs and siLP of CD45.1$^+$ mice in remission phase of asthma, and then adoptively transferred into irradiated CD45.2$^+$ mice (Fig. 2A). Recipient mice were then challenged with HDM intranasally without sensitization as performed on donor mice. Remarkably, flow cytometry analysis of CD45.1$^+$lineage$^-$CD90.2$^+$NK1.1$^-$NKp46$^-$GATA3$^+$ST2$^-$KLRG1$^+$IL-17RB$^+$ ILC2s in CD45.2$^+$ mice demonstrated that only cells from donor siLP gave rise to ST2$^-$KLRG1$^+$IL-17RB$^+$ ILC2s accumulated in

https://doi.org/10.1038/s41467-024-52252-2

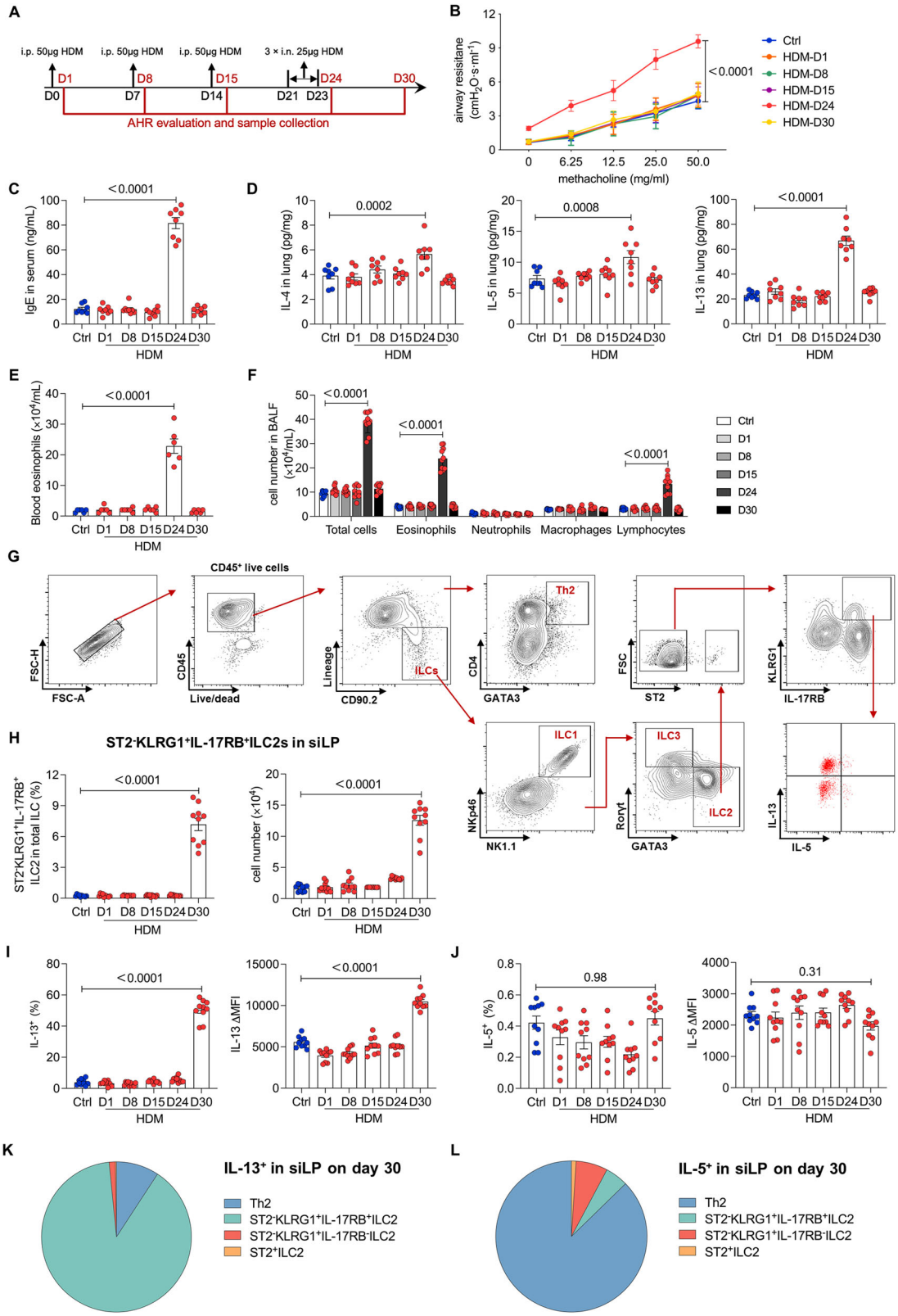

recipient lungs (Fig. 2B–E). Asthmatic changes, as evidenced by elevated IL-13 production, serum IgE level, thickened bronchial wall and inflammatory cell infiltration, were observed in the mice transplanted with siLP-derived cells (Fig. 2F–H). Among these, rapid elevation of IgE might be regulated by high levels of IL-13-induced direct IgE class switching instead of sequential switching from IgM via IgG to IgE[25,26]. Taken together, we tentatively concluded that ST2⁻KLRG1⁺IL-17RB⁺ ILC2s originated from those in siLP in remission might subsequently accumulate in lungs upon another allergen exposure and mediate asthma relapse.

ST2⁻KLRG1⁺IL-17RB⁺ ILC2s circulate and move between airway and siLP during asthma progress

ILC2s are generally considered as tissue-resident cells, but recently Huang and colleagues[20] defined KLRG1^{high} iILC2s as circulating cells, with the ability to migrate in vivo and mediate host defense against

Fig. 1 | Lineage$^-$CD90.2$^+$NK1.1$^-$NKp46$^-$Rorγt$^-$GATA3$^+$ST2$^-$KLRG1$^+$IL-17RB$^+$ ILC2s with IL-13-producing capability accumulated in siLP in asthma remission. **A** Flow diagram of the i.p. HDM sensitization model. Challenge phase: D24, Remission phase: D30. **B** Airway resistance of mice was determined on day 1 (D1), D8, D15, D24 and D30 under methacholine (0, 6.25, 12.5, 25 and 50 mg/mL in PBS) stimulation. **C** Serum IgE ($n = 8$), **D** lung IL-4, IL-5 and IL-13 ($n = 8$), **E** eosinophils in peripheral blood ($n = 6$), and **F** cytology of bronchoalveolar lavage fluid (BALF) ($n = 10$) were determined at indicated time points. **G** Gating strategy. In live CD45$^+$ lymphocytes, Th2s are defined as CD4$^+$GATA3$^+$, and total ILC2s are defined as lineage$^-$CD90.2$^+$NK1.1$^-$NKp46$^-$Rorγt$^-$GATA3$^+$. **H** Kinetics of the frequency and number of ST2$^-$KLRG1$^+$IL-17RB$^+$ ILC2 subset in the lamina propria of small intestines (siLP) ($n = 10$). **I**, **J** IL-13$^+$ percentage and MFI **I** and IL-5$^+$ percentage and MFI **J** of ST2$^-$KLRG1$^+$IL-17RB$^+$ ILC2s in siLP after stimulation with PMA, ionomycin, brefeldin A and monensin. **K**, **L** Pie charts of IL-13$^+$ **K** and IL-5$^+$ **L** cell populations in siLP in remission under stimulation ($n = 10$). Mice in control group (Ctrl) were treated with corresponding volume of sterile normal saline. Data points are individual mice pooled from three independent experiments for all panels. Data are shown as the mean ± SD. Statistical comparisons were performed using unpaired one-way ANOVA with Dunnett's test except in **B** and **F** using unpaired two-way ANOVA. *p* values are shown on the graphs. Source data are provided as a Source Data file.

infection of the hookworm *N. brasiliensis*. We next tried to verify that ST2$^-$KLRG1$^+$IL-17RB$^+$ ILC2s found in siLP in asthma remission were circulating cells utilizing a parabiotic mice model (Fig. 3A, B and Figs S5 and S6). For this, CD45.1$^+$ and irradiated CD45.2$^+$ mice were surgically connected to generate parabiotic partners sharing blood circulation. CD45.1$^+$ mice were subsequently exposed to HDM to induce asthmatic changes. In remission, the changes of CD45.1$^+$ST2$^-$KLRG1$^+$IL-17RB$^+$ ILC2s in CD45.1$^+$ mouse and its CD45.2$^+$ counterpart was analyzed. In line with our previous findings, ST2$^-$KLRG1$^+$IL-17RB$^+$ ILC2s in siLP of CD45.1$^+$ mice were markedly increased (Fig. S5E). Notably, CD45.1$^+$ST2$^-$KLRG1$^+$IL-17RB$^+$ ILC2s were also detected to be elevated in siLP in CD45.2$^+$ littermates, indicating that this particular ILC2 subset was circulating cells. In contrast, negligible ST2$^+$ ILC2s from CD45.1$^+$ mouse was found in its CD45.2$^+$ counterpart (Fig. S6A), which suggested that the ST2$^+$ subset was tissue-resident as reported before. In addition, despite the existence of CD45.1$^+$ST2$^-$KLRG1$^+$IL-17RB$^-$ subset in CD45.2$^+$ mice, no significant changes of them were found in all sites (Fig. S6B), suggesting a specific role of ST2$^-$KLRG1$^+$IL-17RB$^+$ ILC2s during asthma remission.

Recruitment of lymphocytes from the circulation into mucosal tissues requires the engagement of adhesion molecules and their corresponding vascular ligands. Similar to adaptive immune cells, ILCs are reported to express different trafficking receptors, which further contributes to the characterization of their subsets[27–30]. ILC1s and ILC3s in mesenteric LN undergo a retinoic acid-dependent homing receptor switch from CCR7 to CCR9 and α4β7 to traffic to the gut. In contrast, the gut-homing property of Lin$^-$NK1.1$^-$CD127$^+$CD90$^+$Sca-1$^+$KLRG1$^+$GATA-3$^+$ ILC2s is programmed in bone marrow[27]. To further confirm and gain mechanistic insight into the migration of ST2$^-$KLRG1$^+$IL-17RB$^+$ ILC2s between lungs and siLP during asthma process, we performed in vivo imaging and analyzed the potential molecular mechanism of ST2$^-$KLRG1$^+$IL-17RB$^+$ ILC2s migration (Fig. 3C–F, Fig. S7). For this, sorted ST2$^-$KLRG1$^+$IL-17RB$^+$ ILC2s were stained with Xenolight DiR, and then injected intravenously into mice at challenge or remission stage, respectively (Fig. 3C). As a result, ST2$^-$KLRG1$^+$IL-17RB$^+$ ILC2s injected into mice under asthma attack accumulated only in lungs, whereas the majority of ST2$^-$KLRG1$^+$IL-17RB$^+$ ILC2s transferred during asthma remission were identified to reside in SI, suggesting that ST2$^-$KLRG1$^+$IL-17RB$^+$ ILC2s might migrate from airway to intestine during asthma relief. Previous studies have demonstrated that CC chemokine receptor 9 (CCR9)- chemokine (C-C motif) ligand 25 (CCL25) and α4β7 integrin-mucosal vascular addressin cell adhesion molecule 1 (MAdCAM-1) served as the main gut-homing signaling for memory T cells[31], promoting us to further investigate the molecule forces driving ST2$^-$KLRG1$^+$IL-17RB$^+$ ILC2s migration to intestine. Indeed, CCR9 and α4β7 integrin were highly expressed on ST2$^-$KLRG1$^+$IL-17RB$^+$ ILC2s in contrast with ST2$^-$KLRG1$^-$ and ST2$^-$KLRG1$^+$IL-17RB$^-$ subsets (Fig. S7A–D). Concurrently, the levels of CCL25 in SI were markedly increased after airway being exposed to allergen (Fig. S7E) while MAdCAM-1 showed negligible changes, suggesting that CCR9/CCL25 axis might be the major player mediating ST2$^-$KLRG1$^+$IL-17RB$^+$ ILC2s homing to intestine. Supportively, in vivo imaging showed that CCX282-B, a selective antagonist of CCR9, restricted the leaving of most ST2$^-$KLRG1$^+$IL-17RB$^+$ ILC2s in lungs of mice whereas the anti-α4β7 monoclonal antibody Etrolizumab did not, indicating a vital role of CCR9/CCL25 in the homing of ST2$^-$KLRG1$^+$IL-17RB$^+$ ILC2s toward SI (Fig. 3C). Previous study has shown that IL-13 stimulates the expression of chemotactic factors such as CCL25[32]. In line with type 2 cytokines in lungs of asthmatic mice, serum IL-13 and IL-5 increased after airway exposure of HDM, and subsequently decreased in remission (Fig. S8A, B). To determine if IL-13/IL-5 induce CCL25 expression, mixed cells were isolated from SI and treated with recombinant IL-5 and/or IL-13 (Fig. S8C, D). As a result, IL-13 markedly stimulated CCL25 while IL-5 showed negligible effect. In addition, MAdCAM-1 was not affected by both cytokines. These data preliminarily suggested a role of elevated serum IL-13 in inducing intestinal CCL25 production, which helps to explain how CCR9$^+$ST2$^-$KLRG1$^+$IL-17RB$^+$ ILC2s traffic to SI in pathological process of asthma.

In addition, substantial amounts of ST2$^-$KLRG1$^+$IL-17RB$^+$ ILC2s appeared in lungs but not SI when mice were re-exposed to HDM (relapse), further corroborating the in vivo trafficking of ST2$^-$KLRG1$^+$IL-17RB$^+$ ILC2s during asthma relapse as we speculated before. And as evidenced by DiR intensity, ST2$^-$KLRG1$^+$IL-17RB$^+$ ILC2s also proliferated in lungs upon another allergen stimulation. The G protein–coupled sphingosine 1-phosphate (S1P)/S1PR signaling pathway has been reported to be indispensable for KLRG1^{high} iILC2s exit from tissues to lymph[20]. Consistently, we found that S1P expressed highly in the plasma of mice during asthma recurrence (Fig. 3D). Treatment of FTY720, the S1P signaling-specific antagonist, sharply reduced the amount of ST2$^-$KLRG1$^+$IL-17RB$^+$ ILC2s in lungs (Fig. 3E) as the consequence of blocking ST2$^-$KLRG1$^+$IL-17RB$^+$ ILC2s migration from siLP to circulation. Considering that S1P is a shared signal to regulate the migration of several immune cells including T cells, dendritic cells, macrophages, etc., we speculate that the restriction of ST2$^-$KLRG1$^+$IL-17RB$^+$ ILC2s might partially contribute to limited asthmatic responses including pulmonary pathological changes and IL-13 overexpression (Fig. 3F, G).

In aggregate, these data indicated that ST2$^-$KLRG1$^+$IL-17RB$^+$ ILC2s, partially at least driven by CCR9 and S1P signaling, migrated between airway and siLP during asthma relief or relapse.

ST2$^-$KLRG1$^+$IL-17RB$^+$ ILC2s mediate allergen- or IL-25-induced asthma relapse independent of adaptive immune cells

When ST2$^-$KLRG1$^+$IL-17RB$^+$ ILC2s were restricted within siLP during secondary allergen exposure, airway inflammation was markedly dampened as we observed in Fig. 3F, G. Hence, we further analyzed the pathological significance of ST2$^-$KLRG1$^+$IL-17RB$^+$ ILC2s migration during recurrent asthma. To this end, the monoclonal antibody neutralizing KLRG1 was injected intraperitoneally to the established asthmatic model on wild type (WT) or *Rag1*$^{-/-}$ mice, which lacked mature T and B lymphocytes (Fig. 4A). For WT mice, HDM exposure stimulated the expansion of ST2$^-$KLRG1$^+$IL-17RB$^+$ ILC2s in lungs, which was significantly reversed by KLRG1 neutralization (Fig. 4B). In parallel, IL-13, the major effector cytokine produced by ST2$^-$KLRG1$^+$IL-17RB$^+$ ILC2s as we demonstrated in Fig. 1, was substantially decreased in lungs of mice receiving KLRG1 mAb (Fig. 4C). Also, allergen- mediated AHR and histological changes were markedly alleviated upon KLRG1

https://doi.org/10.1038/s41467-024-52252-2

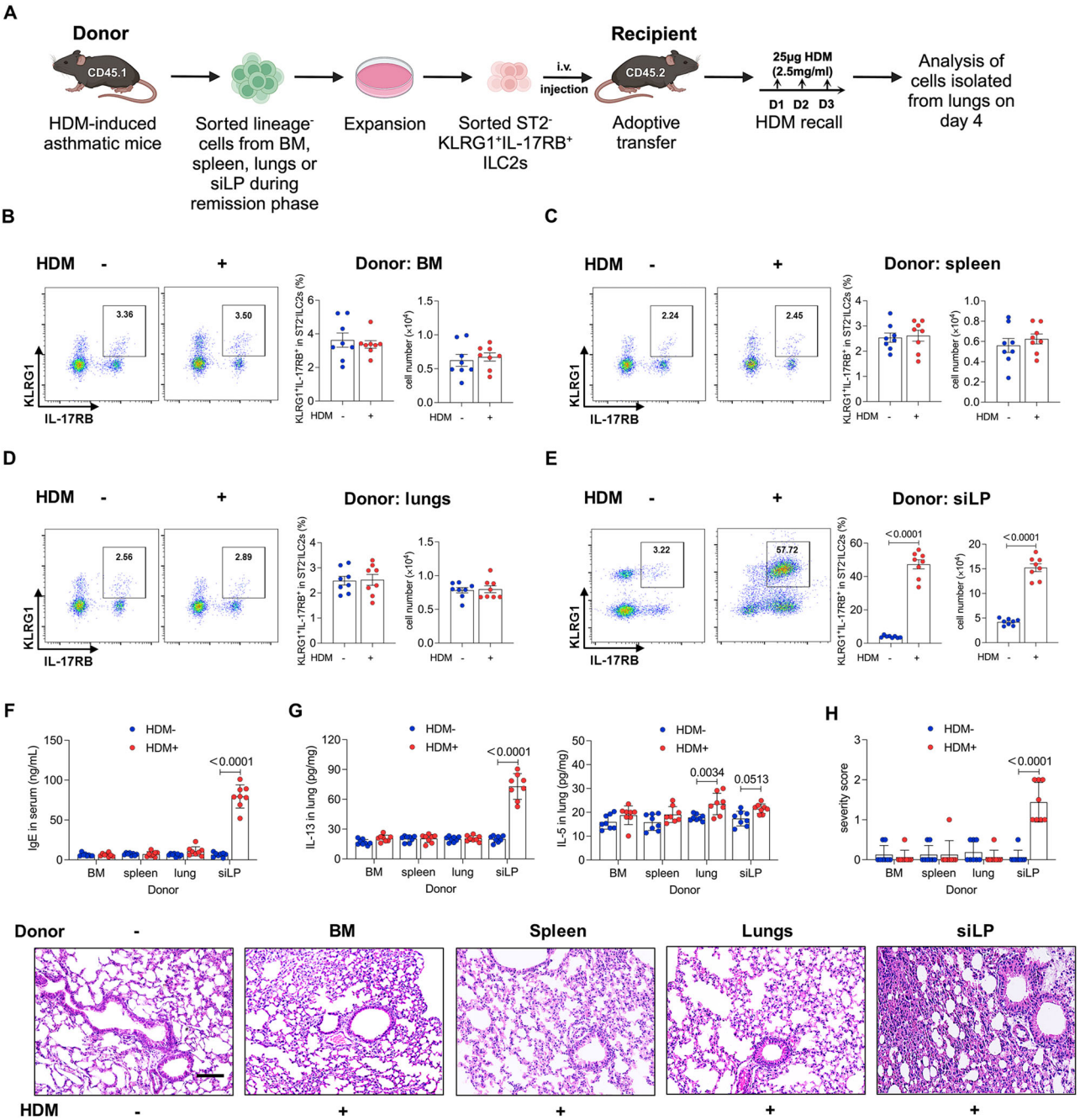

Fig. 2 | siLP was the source of ST2$^-$KLRG1$^+$IL-17RB$^+$ ILC2s accumulated in lungs that mediated recurrence of airway inflammation. A Donor CD45.1$^+$ mice were sensitized and challenged with HDM follow the i.p. HDM sensitization model protocol. On day 30 (remission), lineage-negative cells were isolated from bone marrow (BM), spleen, lungs and siLP, respectively and cultured in vitro for expansion. Subsequently, 5×10^5 CD45$^+$lineage$^-$CD90.2$^+$NK1.1$^-$NKp46$^-$ST2$^-$KLRG1$^+$IL-17RB$^+$ ILC2s were sorted and injected into the irradiated CD45.2$^+$ mice via tail vein. Recipient CD45.2$^+$ mice were then treated with 25 μg HDM intranasally for 3 times once daily. 24 hours later, single cells in lungs were prepared for flow cytometry analysis. **B**–**E** Representative plots and statistical results (bar graph) showing the percentages and the numbers of ST2$^-$KLRG1$^+$IL-17RB$^+$ ILC2s at lungs in mice that received cells derived from **B** BM, **C** spleen, **D** lungs, or **E** siLP, respectively. **F**, **G** IgE levels in serum **F** and IL-13 and IL-5 protein levels in lungs (**G**) of recipient mice in each group were detected by ELISA. **H** Histological scores and representative images of lungs of recipient mice by hematoxylin-eosin staining. Magnification: ×200, scale bar = 100 μm. Results are representative of three independent experiments. Means ± SD from 8 mice each group. Statistical comparisons were performed using unpaired, two-sided Welch's t-test except in **F**–**H** using unpaired two-way ANOVA. *p* values are shown on the graphs. Source data are provided as a Source Data file. Fig. 2A Created with BioRender.com released under a Creative Commons Attribution-NonCommercial-NoDerivs 4.0 International license https://creativecommons.org/licenses/by-nc-nd/4.0/deed.en.

inhibition (Fig. 4D, E). More importantly, similar trend of these changes was observed in *Rag1*$^{-/-}$ mice, suggesting that KLRG1-expressing innate cells were capable of mediating asthmatic responses without the contribution of T and B cells. To further confirm if ST2$^-$KLRG1$^+$IL-17RB$^+$ ILC2s were the pivotal players in this process, ST2$^-$KLRG1$^+$IL-17RB$^+$ ILC2s isolated from siLP of HDM-stimulated *Rag1*$^{-/-}$ mice were treated with KLRG1 mAb or isotype IgG in vitro, followed by adoptive transfer into *Rag1*$^{-/-}$ mice pre-treated with anti-CD90.2 (ILC depleted) via tail vein (Fig. 4F). As portrayed in Fig. 4G–J, ST2$^-$KLRG1$^+$IL-17RB$^+$ ILC2s substantially expanded after HDM or IL-25 exposure, and asthmatic responses were observed in recipient mice. In contrast, KLRG1 mAb-treated cells did not induce similar responses in recipient mice,

https://doi.org/10.1038/s41467-024-52252-2

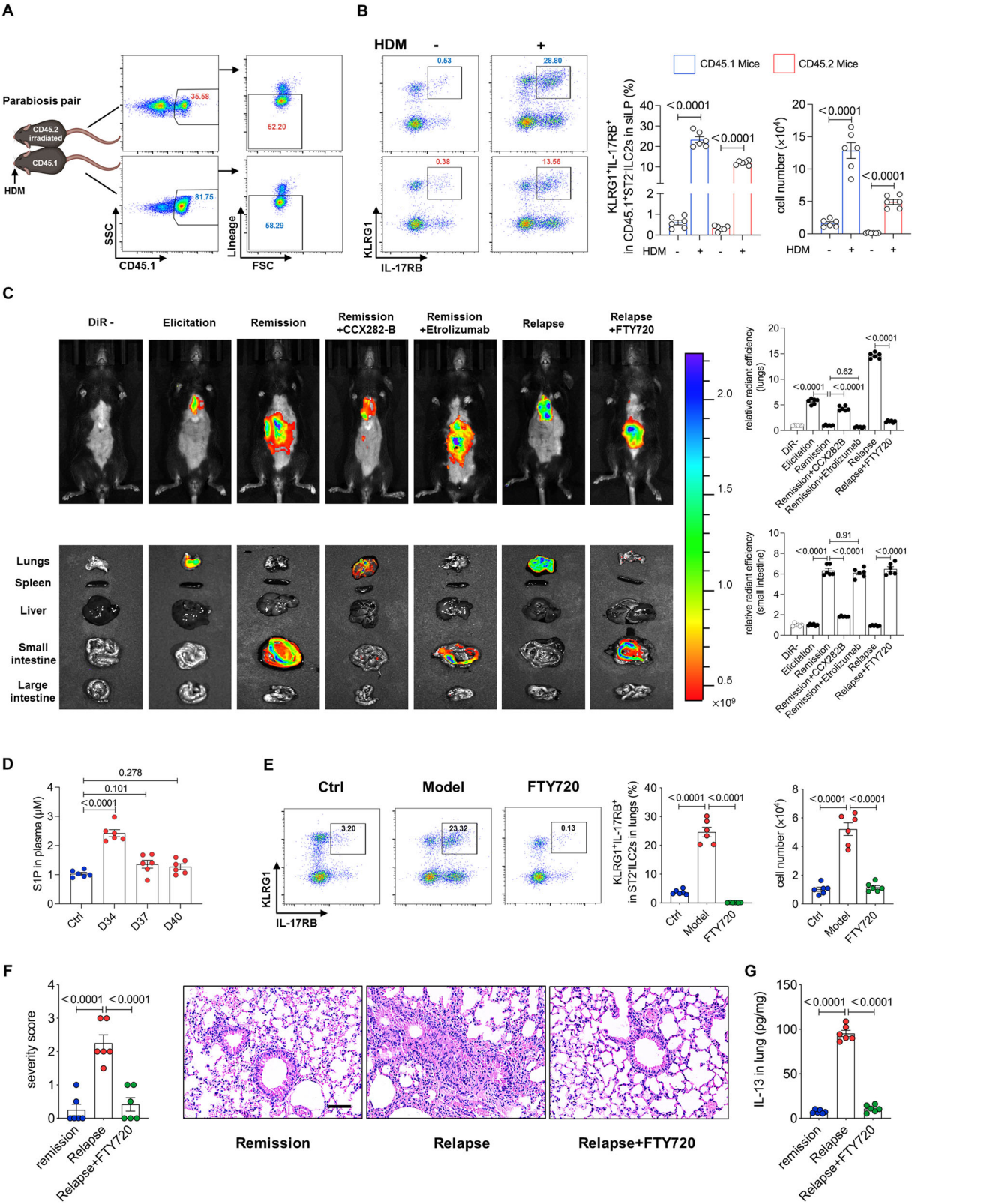

indicating that these transferred antigen- non-specific ST2$^-$KLRG1$^+$IL-17RB$^+$ ILC2s were sufficient to mediate asthmatic inflammation independent of adaptive immune cells or pre-existing ILC2s. Combined with our previous results, it is tentatively proposed that siLP-derived ST2$^-$KLRG1$^+$IL-17RB$^+$ ILC2s rapidly accumulated in lungs through circulation to mediate immune responses, leading to more severe and quicker asthma relapse.

Mice ST2$^-$KLRG1$^+$IL-17RB$^+$ ILC2s in siLP possess memory-like characteristics after the resolution of asthmatic responses

Our data indicate that ST2$^-$KLRG1$^+$IL-17RB$^+$ ILC2s with IL-13- producing potential accumulate in siLP during steady state of asthma and these specific subset of ILC2s are able to migrate to airway to induce recurrent asthma-like responses upon allergen or IL-25 exposure. We propose that siLP ST2$^-$KLRG1$^+$IL-17RB$^+$ ILC2s might serve as

Fig. 3 | Circulating ST2$^-$KLRG1$^+$IL-17RB$^+$ ILC2 subset migrated between airway and siLP in HDM-induced asthma. A CD45.1$^+$ and irradiated CD45.2$^+$ mice were surgically jointed from olecranon to knee joint and recovered for 4 weeks to establish blood chimerism. Subsequently, CD45.1$^+$ mice were treated with HDM as Fig. 1A. **B** The percentages and the numbers of ST2$^-$KLRG1$^+$IL-17RB$^+$ ml-ILC2s in siLP of CD45.1$^+$ and CD45.2$^+$ were analyzed on day 30. Cells were gated on CD45.1$^+$lineage$^-$CD90.2$^+$NK1.1$^-$NKp46$^-$GATA3$^+$. For in vivo imaging experiments, mice were treated with HDM to establish the asthma relapse model as portrayed in Fig. S4. **C** On day 30 (remission), ST2$^-$KLRG1$^+$IL-17RB$^+$ ILC2s were sorted from siLP and stained with 5 mM Xenolight DiR, and then injected intravenously (5×10^5 cells/each) into various groups of mice. Specifically, mice in DiR- group were injected with unstained cells. For the remission + CCX282-B group, recipient mice resting from asthma symptoms were treated with the CCR9 antagonist CCX282-B at 50 mg/kg (daily injection subcutaneously) from day 24 to day 30. For the remission + Etrolizumab group, recipient mice resting from asthma symptoms were treated with the anti-α4β7 monoclonal antibody Etrolizumab at 5 mg/kg (injection intravenously) on day 24, 26, 28 and 30. For the relapse group, mice in remission were injected with DiR-stained cells, followed with treatment of HDM at 50 μg intranasally for 2 times once per hour. Mice in the relapse + FTY720 group received intravenous injection of FTY720 along with 2-time intranasal administration of HDM. Mice in all groups were imaged 2 hours post cell injection, and organs including lungs, spleen, liver, SI and large intestine were then rapidly harvested and imaged. **D** S1P expression in plasma collected from mice post asthma relapse (D34, D37 and D40) was measured by ELISA. The S1P signaling antagonist FTY720 was administered intraperitoneally to asthmatic mice on days 31 to 33 for 3 times. **E** The percentages and the numbers of ST2$^-$KLRG1$^+$IL-17RB$^+$ ILC2s in lungs were detected on D34. **F** Histological examination of lungs by hematoxylin-eosin staining. Magnification: ×200, scale bar = 100 μm. **G** Protein levels of IL-13 in lungs was detected by ELISA. Results are representative of three independent experiments. Means ± SD from 6 mice for each group. Statistical comparison was conducted using unpaired, two-sided Welch's *t* test for **B** and unpaired one-way ANOVA with Dunnett's test for the rest. *p* values are shown on the graphs. Source data are provided as a Source Data file. Fig. 3A Created with BioRender.com released under a Creative Commons Attribution-NonCommercial-NoDerivs 4.0 International license https://creativecommons.org/licenses/by-nc-nd/4.0/deed.en.

immunological memory cells as adaptive immune cells with great potential to induce asthma recurrence. Considering that immune memory cells are generally long-lived[11], we then analyzed the persistence of ST2$^-$KLRG1$^+$IL-17RB$^+$ ILC2s in siLP after HDM exposure (Fig. 5A). As portrayed in Fig. 5B, C, the level of ST2$^-$KLRG1$^+$IL-17RB$^+$ ILC2s was substantially escalated and remained high in siLP up to 90 days after challenge. In contrast, the abundance of ST2$^-$KLRG1$^+$IL-17RB$^+$ ILC2s in PBMC, lungs and mesenteric LN increased 24 hrs after challenge and declined to similar level of control group (Fig. S9A–E). We then intranasally administered the nuclear-staining agent, bromodeoxyuridine (BrdU), into mice with HDM challenge from day 21 to day 23 (Fig. 5D). Intriguingly, results showed that most siLP ST2$^-$KLRG1$^+$IL-17RB$^+$ ILC2s (74.9 ± 1.4%) incorporated BrdU (Fig. 5D), and BrdU$^+$ST2$^-$KLRG1$^+$IL-17RB$^+$ ILC2s were detected up to 90 days after challenge, suggesting this ILC2 subset as a population endow longevity the specific characteristic of immunological memory cells. Similar results were found in the i.n. HDM sensitization model with only airway exposure of HDM that BrdU$^+$ST2$^-$KLRG1$^+$IL-17RB$^+$ ILC2s could be detected 60 days after last HDM exposure (Fig. S10). These data demonstrated that high amount of long-lived ST2$^-$KLRG1$^+$IL-17RB$^+$ ILC2s in siLP during asthma remission was from the survived cells in airway, as BrdU was only administered intranasally.

Memory immunological cells like T_{mem} display superior proliferation capacity and remain poised to rapidly elaborate effector functions upon pathogen re-exposure[33]. We then used recombinant mouse IL-33 and IL-25 as alarmins to stimulate three siLP-sorted ST2$^-$ILC2 subpopulations including KLRG1$^-$, KLRG1$^+$IL-17RB$^-$ and KLRG1$^+$IL-17RB$^+$ during asthma remission (herein referred as AR-KLRG1$^-$, AR-KLRG1$^+$IL-17RB$^-$ and AR-KLRG1$^+$IL-17RB$^+$) and ST2$^-$KLRG1$^+$IL-17RB$^+$ ILC2 sorted from siLP of naive WT mice (herein referred as naive-KLRG1$^+$IL-17RB$^+$) (Fig. 5E). After stimulation, 90.2% of AR-KLRG1$^+$IL-17RB$^+$ILC2s were Ki-67-positive, in sharp contrast with naive-KLRG1$^+$IL-17RB$^+$, AR-KLRG1$^-$ and AR-KLRG1$^+$IL-17RB$^-$ subsets (Fig. 5F). Considering of similar trend was found in absolute cell number and expansion analysis (Fig. 5G, H), we confirmed that ST2$^-$KLRG1$^+$IL-17RB$^+$ ILC2s in siLP of mice during asthma remission endowed strong proliferation and expansion capability. Moreover, AR-KLRG1$^+$IL-17RB$^+$ ILC2s retained great potential of producing IL-13 whereas only 3.43% of naive-KLRG1$^+$IL-17RB$^+$ and 4.85% of AR-KLRG1$^+$IL-17RB$^-$ were IL-13$^+$ and AR-KLRG1$^-$ showed negligible cytokine-producing capability after stimulation (Fig. 5I). The percentage of IL-5- producing cells, by contrast, all ranged from 1.16 % to 3.42% for these four subsets with or without alarmins treatment. As reported[19], KLRG1^{high}iILC2s produce amount of IL-17 in contrast with siLP AR-KLRG1$^+$IL-17RB$^+$ ILC2s sorted during asthma remission, indicating them as distinct phenotypes (Fig. S11).

Taken these data into consideration, this particular AR-ST2$^-$KLRG1$^+$IL-17RB$^+$ ILC2s accumulated in siLP were distinct from other subpopulations of ILC2s at the same location during remission phase. Furthermore, naive-ST2$^-$KLRG1$^+$IL-17RB$^+$ ILC2s did not endow similar properties, which suggest that AR-ST2$^-$KLRG1$^+$IL-17RB$^+$ ILC2s in siLP after asthma resolves serve as "trained" or immunological memory cells contributing to relapse. Hence, we herein define AR-ST2$^-$KLRG1$^+$IL-17RB$^+$ ILC2s as long-lasting memory-like ILC2s (ml-ILC2s) based on the conception proposed before[11,14].

Tcf7 and *Tox* are essential for the memory-like functions of ml-ILC2s

For a further depth view of memory-induction of ml-ILC2s in mice asthma remission, we then analyzed the expression of various genes which are previously reported being related with immunological memory-induction, cell residency and activation. As a result, naive-ST2$^-$KLRG1$^+$IL-17RB$^+$, AR-ST2$^-$KLRG1$^-$, AR-ST2$^-$KLRG1$^+$IL-17RB$^-$ and AR-ST2$^-$KLRG1$^+$IL-17RB$^+$ (ml-ILC2s) showed distinct transcriptional hallmarks (Fig. 6).

Several genes implicated in exhaustion and memory-induction were differentially expressed in ml-ILC2s, e.g., down-regulation of *Pdcd1* and up-regulation of *Tox* and *Tcf7* (Fig. 6A, Fig. S12A). By encoding programmed death 1 (PD-1), *Pdcd1* induces a cascade of intracellular signaling that results in T cell inhibition and exhaustion[34]. Activated ILC2s are recognized to express high level of PD-1[35,36]. PD-1 alters cell metabolism and function of IL-33-induced pulmonary Lin$^-$ST2$^+$CD127$^+$ ILC2s, and PD-1 agonist limits the activation and proliferation of these ILC2s[35]. Similarly, PD-1 suppresses the effector function of Lin$^-$CD45$^+$CD127$^+$GATA3$^+$KLRG1$^+$ ILC2s against helminthic infection via inhibiting signal transducer and activator of transcription 5 (STAT5) signaling[36]. In our study, ST2$^-$KLRG1$^+$IL-17RB$^+$ ml-ILC2s display relatively lower expression of *Pdcd1*, raising the possibility that these allergen-primed ml-ILC2s in siLP have undergone PD-1-induced contraction and are at steady state during asthma remission. *Tcf7*, which encodes T cell factor 1 (TCF-1), a high-mobility group (HMG) box transcription factor that plays a pivotal role in the differentiation and survival of memory CD8$^+$ T cells[37,38]. *Tox* encodes thymocyte selection-associated high-mobility group box protein TOX (TOX), a member of the high-mobility group transcription factors[39]. Several studies suggest that TOX is not exclusively associated with T cell exhaustion. To illustrate, Yao et al. [40]. report that TOX is required for the programming of progenitor-like CD8$^+$ T cells in chronic infection. Sekine and colleagues[41] find that most circulating effector memory CD8$^+$ T cells also express TOX. Our data indicate that ml-ILC2s express high mRNA levels of *Tcf7* and *Tox*, suggesting TCF-1 and TOX signaling might be

https://doi.org/10.1038/s41467-024-52252-2

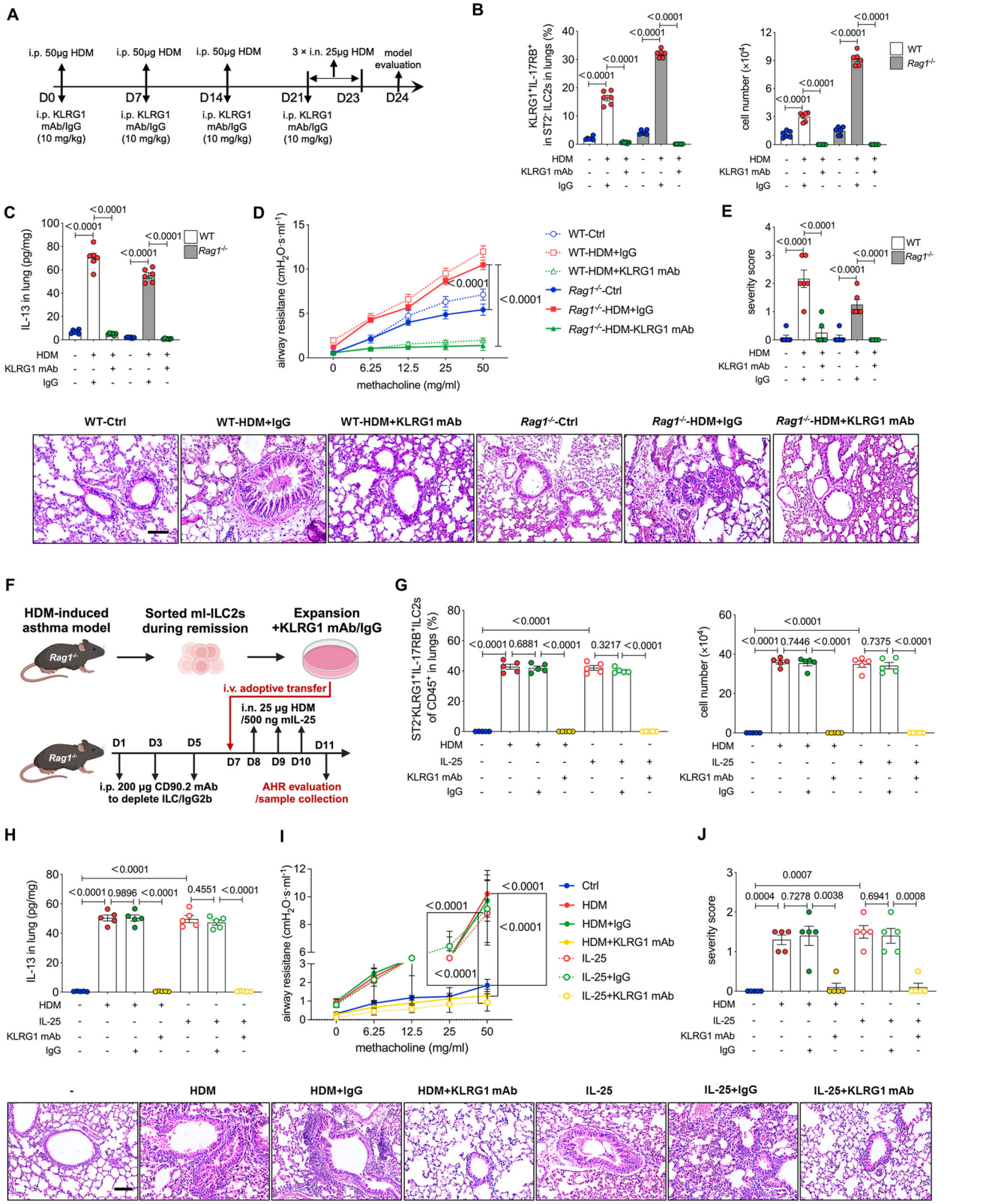

required for memory development of ml-ILC2s during asthma relief. *Bach2 (BTB and CNC homology, basic leucine zipper transcription factor 2)*, *Myb (myeloblastosis oncogene)* and *Id3 (inhibitor of DNA binding 3)* are considered to be the transcriptional factors to promote memory T cell formation beside *Tcf7* and *Tox*[42–46], but negligible difference of their expression levels was observed in ml-ILC2s. In addition, several key regulators including *Maf (MAF bZIP transcription factor)*, *Fhl2 (four and a half LIM domains 2)*, *Zeb1 (zinc finger E-box binding homeobox 1)*, *Fosb (FBJ osteosarcoma oncogene B)*, *Runx1 (runt related transcription factor 1)*, *Nr4a2 (nuclear receptor subfamily 4, group A, member 2)*, and *Mpp7 (membrane protein, palmitoylated 7 (MAGUK p55 subfamily member 7))* have been reported to be associated with memory-like properties of papain- and *Aspergillus*-primed ILC2s[16,47]. However, our result showed that the expression levels of these genes were not

Fig. 4 | siLP-derived ST2$^-$KLRG1$^+$IL-17RB$^+$ ILC2s mediated asthmatic responses independent of adaptive immune cells. A WT or *Rag1*$^{-/-}$ mice were stimulated with HDM, and anti-KLRG-1 mAb or isotype IgG were administered intraperitoneally as indicated. **B** The percentage and the number of CD45$^+$ lineage$^-$CD90.2$^+$NK1.1$^-$NKp46$^-$GATA3$^+$ST2$^-$KLRG1$^+$IL-17RB$^+$ ILC2s in lungs were analyzed on day 24. **C** Pulmonary IL-13 was detected by ELISA. **D** Airway resistance was measured under stimulation of methacholine. **E** Pulmonary histological changes were observed by hematoxylin-eosin staining. Magnification: ×200, scale bar = 100 μm. **F** *Rag1*$^{-/-}$ mice were stimulated with HDM, and CD45$^+$lineage$^-$ CD90.2$^+$ST2$^-$KLRG1$^+$IL-17RB$^+$ ILC2s were sorted from siLP on D30. In vitro culturing cells were treated with anti-KLRG1 mAb or isotype control, and then adoptively transferred into untreated ILC2 depleted (anti-CD90.2 mAb or isotype control) *Rag1*$^{-/-}$ mice via tail vein (5×10^5 cells/mouse). Recipient mice were intranasally treated (i.n.) with 25 μg HDM or 500 ng recombinant IL-25 for 3 consecutive days. **G** The percentage and the number of CD45$^+$lineage$^-$CD90.2$^+$NK1.1$^-$NKp46$^-$GATA3$^+$ ST2$^-$KLRG1$^+$IL-17RB$^+$ ILC2s in lungs. **H**, **I** IL-13 level in lungs homogenates **H** and airway resistance **I** was measured. **J** Pulmonary histological changes were analyzed. Magnification: ×200, scale bar = 100 μm. Results are representative of three independent experiments. Data was shown as Means ± SD. $n = 6$ in all panels except for $n = 3$ in **D** and **I**. Statistical comparison was conducted using unpaired, two-sided Welch's t test, except in (**D**) and (**I**) using unpaired two-way ANOVA with the Bonferroni posttest to analyze dose response to methacholine. p values are shown on the graphs. Source data are provided as a Source Data file. Fig. 4F Created with BioRender.com released under a Creative Commons Attribution-NonCommercial-NoDerivs 4.0 International license https://creativecommons.org/licenses/by-nc-nd/4.0/deed.en.

markedly changed (Fig. 6A, Fig. S12A), raising the possibility that they are not the key regulators in memory-induction of ml-ILC2s. These transcriptional differences suggest an exclusive role of ST2$^-$KLRG1$^+$IL-17RB$^+$ ml-ILC2s in asthma relapse.

We then knockdown *Tcf7* and *Tox* to evaluate the regulatory roles of them in memory-like functions of ml-ILC2s. For in vitro cultures, levels of target mRNAs and proteins of ml-ILC2s were markedly decreased after transfection as evidenced by q-PCR and flow cytometry analysis (Fig. S13A–D). In addition, ml-ILC2s expanded and secreted amount of IL-13 after alarmins treatment for 8 consecutive days, which was notably inhibited by *Tcf7* and *Tox* interference (Fig. 6B, C). Besides, si*Tcf7* and si*Tox* markedly downregulated the mRNA levels of *Klrg1, Il-17rb, Il1rl1, Il2ra, Il7r, Il13, Gata3, Ccr9* and *S1pr1* of ml-ILC2s (Fig. 6D and Fig. S14). We found that *Tcf7* and *Tox* knockdown notably decreased the expression of CCR9 and S1PR1 of ml-ILC2s (Fig. 6E, F). Next, we employed BrdU to evaluate the longevity and migration of ml-ILC2s during asthma development when *Tcf7* or *Tox* was knockdown (Fig. 6G). About 80% of ST2$^-$KLRG1$^+$IL-17RB$^+$ ml-ILC2s was BrdU-positive in siLP during asthma remission (D61), which was sharply decreased by si*Tcf7* or si*Tox* (Fig. 6H). Furthermore, upon asthma relapse, we found that about 70% of ST2$^-$KLRG1$^+$IL-17RB$^+$ ml-ILC2s in lungs was BrdU-labeled whereas the average percentages were only 4.2% and 11.4% when *Tcf7* and *Tox* were interfered, respectively (Fig. 6I). These data suggested that *Tcf7* and *Tox* were pivotal for the migrating capability and/or long-lasting of ml-ILC2s. We then injected in vivo siRNAs via tail vein of *Rag1*$^{-/-}$ mice to knockdown *Tcf7* and *Tox* and adoptively transferred ml-ILC2s before secondary asthma attack (Fig. 6J). As portrayed in Fig. 6K–M, another 3-day airway exposure of HDM rapidly induced AHR, elevated protein levels of IL-13 in lungs and inflammatory cell infiltration and thickened bronchial walls in *Rag1*$^{-/-}$ mice. Both in vivo si*Tcf7* and si*Tox* prominently alleviated these asthmatic responses, which could be inverted by subsequent adoptive transfer of cultured ml-ILC2s but not those cells pre-transfected by siRNAs. Collectively, these data demonstrated that *Tcf7* and *Tox* were key factors to regulate the memory-like properties of ml-ILC2s including longevity, hyperresponsiveness and inter-organ migration during asthma progress.

Human CD45$^+$lineage$^-$CRTH2$^+$CD127$^+$GATA3$^+$ST2$^-$KLRG1$^+$IL-17RB$^+$ ILC2s are identical to mice ml-ILC2s

Based on the data acquired from mice models, we have determined that ml-ILC2s possess memory-like characteristics and in vivo trafficking property, orchestrating asthmatic recurrence upon another challenge. To probe if ST2$^-$KLRG1$^+$IL-17RB$^+$ ILC2s persist in asthmatic patients during remission, we collected PBMCs from 15 asymptomatic volunteers with physician-diagnosed asthma, and analyzed the CD45$^+$lineage$^-$CRTH2$^+$CD127$^+$GATA3$^+$ST2$^-$KLRG1$^+$IL-17RB$^+$ ILC2s population within. The results showed that CD45$^+$lineage$^-$CRTH2$^+$CD127$^+$ GATA3$^+$ST2$^-$KLRG1$^+$IL-17RB$^+$ ILC2s in circulation remained higher in asthmatic participants compared with healthy control (Fig. 7A, B). Moreover, over 60% of ST2$^-$KLRG1$^+$IL-17RB$^+$ ILC2s were determined as IL-13- producing subset, whereas negligible changes were identified with IL-5-producing potentiality (Fig. 7C, D). In contrast, KLRG1$^-$ and KLRG1$^+$IL-17RB$^-$ subsets showed no significant changes and possess relatively stronger IL-5-producing potentiality than IL-13 (Fig. S15). These data suggested that human ST2$^-$KLRG1$^+$IL-17RB$^+$ ILC2s maintained pro-inflammatory phenotype despite at asthma remission phase with negligible clinical signs. To further probe if human ST2$^-$KLRG1$^+$IL-17RB$^+$ ILC2s possess memory-like features like we observed in mice models, we sorted the ST2$^-$KLRG1$^+$IL-17RB$^+$ ILC2s from PBMC of healthy donors (marked as H-KLRG1$^+$IL-17RB$^+$) and three subsets of ST2$^-$ ILC2s from human PBMC in asthma remission (marked as A-KLRG1$^-$, A-KLRG1$^+$IL-17RB$^-$ and A-KLRG1$^+$IL-17RB$^+$) and cultured them with stimulation of recombinant human IL-25 and IL-33 (Fig. 7E). Ki-67 staining, changes of cell number and expansion increase confirmed that ST2$^-$KLRG1$^+$IL-17RB$^+$ subset from asthmatic patients retained strong proliferation capability (Fig. 7F–H). In sharp contrast with H-KLRG1$^+$IL-17RB$^+$, A-KLRG1$^-$ and A-KLRG1$^+$IL-17RB$^-$ subsets, A-ST2$^-$KLRG1$^+$IL-17RB$^+$ ILC2s displayed hyper potential of producing IL-13 under stimulation of alarmins (Fig. 7I). In addition, IL-5-producing capability of human A- KLRG1$^+$IL-17RB$^+$ was relatively mild, similar to mice ml-ILC2s (Fig. 7J). As portrayed in Fig. 7K, L, mRNA levels of *PDCD1* decreased and *TOX*, *TCF-7*, *IL2RA*, *IL7R*, *CCR9, S1PR1*, *IL-13* and *GATA3* increased in A-KLRG1$^+$IL-17RB$^+$ ILC2s, suggesting this specific ILC2 subset in circulation of asthmatic patients during remission with identical transcriptional hallmarks to mice memory-like ml-ILC2s. Collectively, these results indicated that CD45$^+$lineage$^-$CRTH2$^+$CD127$^+$ GATA3$^+$ST2$^-$KLRG1$^+$IL-17RB$^+$ ILC2s in peripheral blood of asthmatic patients during remission possess memory-like characteristics, in parallel to ml-ILC2s defined in mice models.

Discussion

Previously, leukocytes like macrophages, NK cells and ILC2s, etc., have been reported to acquire a long-lasting memory-like property, termed "trained immunity"[11]. NK cells acquire memory characteristics after being activated by cytomegalovirus or cytokines, including IL-12, IL-15 and IL-18, suggesting NK cell memory can be antigen-specific or antigen-non-specific. The antigen-specific memory of NK cells is dependent on the Ly49H receptor, which capacitate NK cells to recognize viral antigens[48]. But ILC2 memory has been described as antigen non-specific in several recent studies. Previous study[14] indicates that ST2$^+$ ILC2s activated by intranasal papain or IL-33 persist in lungs and draining mediastinal LN, and respond more vigorously than naive ILC2s to a secondary stimulation, evidenced by BrdU-labeling and type 2 cytokines secretion. Also, lung ST2$^+$ ILC2s, preactivated by the fungal allergen *Aspergillus oryzae* protease, significantly elevate and produce an incredible amount of IL-5 and IL-13 followed by a single intranasal challenge of another allergen papain, suggesting these lung-resident memory ST2$^+$ ILC2s are allergen non-specific[14]. Based on two models of our study, increased Th2s and several ILC2 subsets including ST2$^+$ ILC2s, ST2$^-$KLRG1$^+$IL-17RB$^+$ and ST2$^-$KLRG1$^+$IL-17RB$^-$ were found in HDM (*Der p 1*)-challenged lungs. However, only ST2$^-$KLRG1$^+$IL-17RB$^+$

https://doi.org/10.1038/s41467-024-52252-2

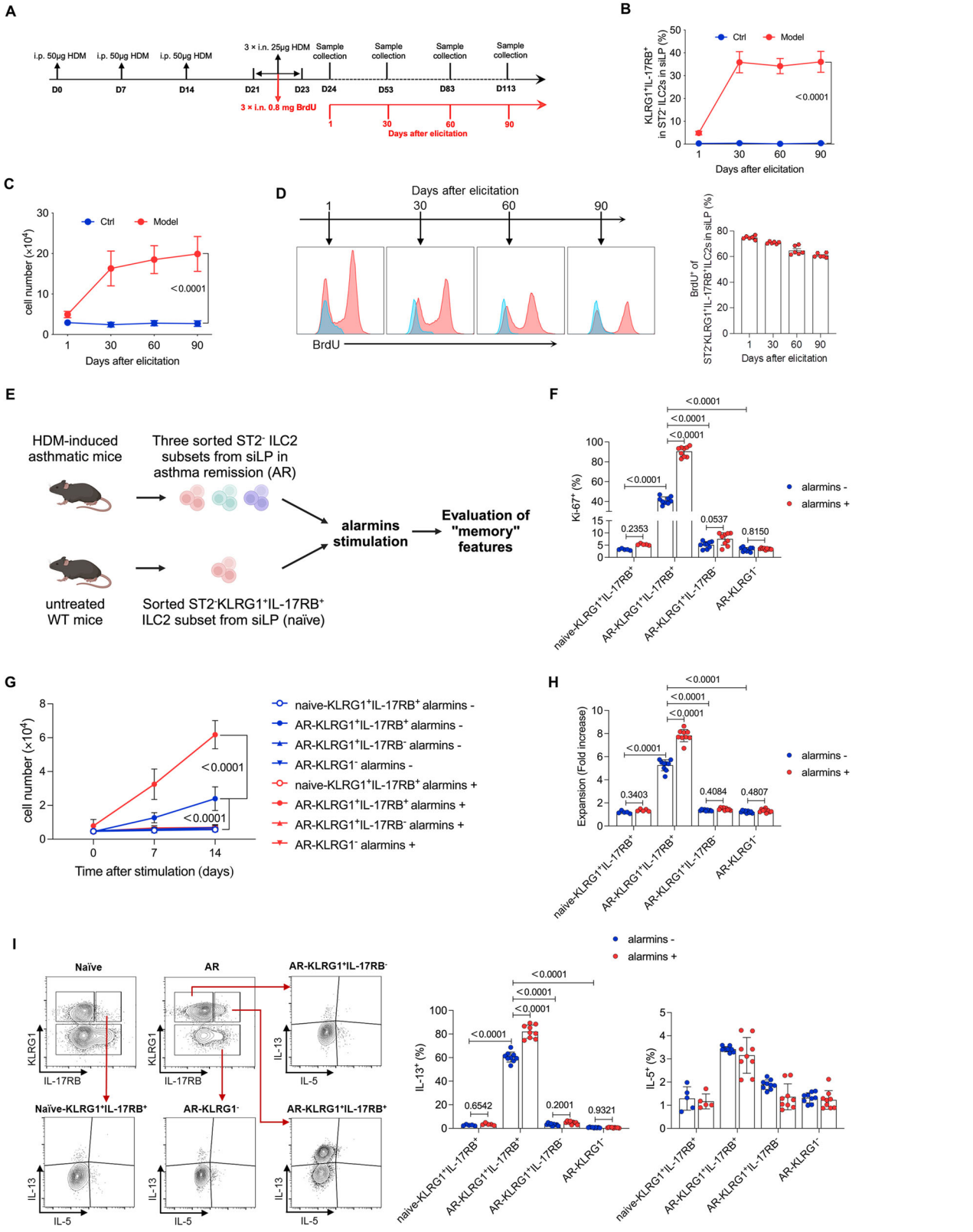

ml-ILC2s accumulated and persisted in distal siLP after asthma resolution whereas Th2s and other ILC2s all decreased. And this particular subset of ml-ILC2s accumulated in siLP during remission phase remain positive for intracellular IL-13. Another airway exposure to HDM or IL-25 resulted in prominently expanded ST2$^-$KLRG1$^+$IL-17RB$^+$ ml-ILC2s in lungs alongside with aggravated asthmatic reponses, raising the possibility that ST2$^-$KLRG1$^+$IL-17RB$^+$ ml-ILC2s might play a key role in orchestrating asthma relapse. Furthermore, airway administration of BrdU resulted in the persistence of BrdU$^+$ ml-ILC2s as long as 90 days (60 days observed on the airway treatment-only HDM mice model) in siLP, indicating that ST2$^-$KLRG1$^+$IL-17RB$^+$ ml-ILC2s acquire longevity, which is one of the characteristics of memory immune cells. Besides, in vitro experiments indicate that sorted siLP ml-ILC2s retain high-potential of proliferation and expansion upon exposure to IL-25 and IL-

Fig. 5 | ST2$^-$KLRG1$^+$IL-17RB$^+$ ILC2s in siLP of mice in asthma remission were endowed with memory-like characteristics. A Flow chart of asthma mice model establishment and sample collection. **B**, **C** On days 21 to 23, BrdU (0.8 mg/mice) was given intranasally. At indicated time points, single-cell suspension was prepared and subjected to flow cytometry analysis; Dynamic changes of the percentage **B** and numbers **C** of CD45$^+$lineage$^-$CD90.2$^+$GATA3$^+$ST2$^-$KLRG1$^+$IL-17RB$^+$ ILC2s in siLP. **D** The proportions of BrdU$^+$ST2$^-$KLRG1$^+$IL-17RB$^+$ ILC2s in siLP of HDM-challenged mice were analyzed by flow cytometry. A control histogram (shaded in blue) was generated using cells from ctrl mice stained with BrdU. **E** During asthma remission (AR) (day 30) of the i.p. HDM sensitization model, three ILC2 subsets including KLRG1$^-$, KLRG1$^+$IL-17RB$^+$ and KLRG1$^+$IL-17RB$^+$ (marked as AR-KLRG1$^-$, AR-KLRG1$^+$IL-17RB$^+$ and AR-KLRG1$^+$IL-17RB$^+$) were purified from the total CD45$^+$lineage$^-$CD90.2$^+$ST2$^-$ cells from siLP. Besides, ST2$^-$KLRG1$^+$IL-17RB$^+$ ILC2s (marked as naive-KLRG1$^+$IL-17RB$^+$ ILC2s) were sorted from siLP of untreated WT mice. Cells were then cultured (5×10^3/well) with 10 ng/mL IL-2 and 20 ng/mL IL-7, and treated with (alarmins +) or without (alarmins-) 200 ng/mL IL-25 and 200 ng/mL IL-33 every other day for 14 days. Subsequently, cells were collected for further analysis. (F-H) Ki-67$^+$ percentage **F**, number (**G**) and fold changes **H** of expansion of cells were determined. **I** Representative plots and statistical results (bar graph) showing the percentages of IL-13$^+$ and IL-5$^+$ of these four ILC2 subsets after stimulation with PMA, ionomycin, brefeldin A and monensin. Data are representative of four independent experiments. Means ± SD; $n = 5$ for the naive-KLRG1$^+$IL-17RB$^+$ group, and $n = 9$ for the other groups. **B**, **C** statistical comparisons were performed using unpaired, two-sided Welch's t test. **F**–**I** unpaired two-way ANOVA with the Bonferroni posttest analysis was performed. p values are shown on the graphs. Source data are provided as a Source Data file. Fig. 5E Created with BioRender.com released under a Creative Commons Attribution-NonCommercial-NoDerivs 4.0 International license https://creativecommons.org/licenses/by-nc-nd/4.0/deed.en.

33. Notably, this ILC2 subset tends to produce IL-13 rather than IL-5 upon challenge, but the underlying mechanism remains to be investigated.

Generally, CD45RA$^-$ memory T cells are divided into CCR7$^-$ effector memory T cells (T_{em}) and CCR7$^+$ central-memory T cells (T_{cm}): the former subsets recirculate and rapidly enter peripheral tissues to mediate inflammatory responses upon another infection while the latter travel to secondary lymphoid organs after infection regressed and can stimulate dendritic cells, B cells and generate a great number of effector cells upon secondary stimulation[49]. Previously, KLRG1^{hi} iILC2s have been demonstrated to possess migrating property from intestine to lungs during *N. brasiliensis* infection[19,20]. The source of the iILC2s migrating to lungs to expulse *N. brasiliensis* is pre-perturbated small intestine (SI), which distinct from the secondary lymphoid tissue-homing, recirculation and subsequent inflamed site-targeting migration processes of memory T cells. Martinez-Gonzalez, I. et al. also reported that ILC2s elevated in the blood and in the liver weeks after activation[14]. naive ILC2s and ST2$^+$ memory ILC2s previously reported are tissue-resident[14,16,50,51]. In our study, observation of kinetic changes and parabiosis study indicated that ST2$^-$KLRG1$^+$IL-17RB$^+$ ml-ILC2s firstly proliferated in airway upon allergen exposure, but subsequently move to peripheral circulation and finally accumulated in siLP in asthma remission. It is intriguing as they are circulating cells, which distinct from those lung-resident memory ST2$^+$ ILC2s as previously reported[14,16]. In addition, adoptive transfer experiments suggested that the large number of ml-ILC2s in lungs upon secondary allergen exposure derived from the cells reside in siLP in asthma remission, which resembles the infected tissue-homing capability of memory T cells. Furthermore, in vivo imaging showed that ml-ILC2s injected into mice upon asthma attack accumulated in lungs whereas those injected into mice during remission were found primarily in SI. In addition, intranasal administration of BrdU during HDM stimulation gave rise to elevated BrdU$^+$ ml-ILC2s in siLP. These data indicated a siLP-homing process of ml-ILC2s after asthma resolution, similar to the secondary lymphoid tissue-homing property of memory T cells.

Collectively, allergen-primed ST2$^-$KLRG1$^+$IL-17RB$^+$ ml-ILC2s are memory immune cells endowed with many of the immunological memory characteristics like memory T cells, among which in vivo migrating capability between lungs and intestine of ml-ILC2s in asthma development is firstly reported in this study. And these data highlight an immune memory cell-like tissue-homing, recirculation, and inflamed site-targeting characteristic of ST2$^-$KLRG1$^+$IL-17RB$^+$ ml-ILC2s during asthma, which distinct from the intestine-lung migration of iILC2s along with the process of helminth intrusion. Critically, we also found that CD45$^+$lineage$^-$CRTH2$^+$CD127$^+$GATA3$^+$ST2$^-$KLRG1$^+$IL-17RB$^+$ ILC2s remain higher in peripheral blood of clinical asthmatic patients even they were asymptomatic in remission phase. These human ST2$^-$KLRG1$^+$IL-17RB$^+$ ILC2s also possessed memory-like features like strong proliferation and IL-13-producing capabilities, in parallel with mice ml-ILC2s we found in experimental models.

Previously studies have shown that ILC2 activation induced by papain can mediate T cell-independent acute allergic inflammation in *Rag*-deficient mice, and *RAR-related orphan receptor alpha* (*Rora*)$^{sg/sg}$ BMT mice deficient for ILC2s fail to develop inflammatory responses, suggesting that ILC2s are pivotal in the generation of type 2 responses[52,53]. We investigated whether ST2$^-$KLRG1$^+$IL-17RB$^+$ ml-ILC2s could induce asthmatic responses independent of adaptive immune cells and pre-existing ILC2s by transferring siLP-derived ml-ILC2s into naive *Rag1*$^{-/-}$ mice pre-treated with anti-CD90.2 and performing intranasal administration of HDM or recombinant IL-25. Results showed that direct allergen stimulation without pre-sensitization resulted in further-expanded ml-ILC2s in lungs, and asthmatic responses including higher IL-13 level and worsen AHR. In addition, ml-ILC2s isolated from siLP of HDM-primed *Rag1*$^{-/-}$ mice led to similar changes in mice received IL-25, indicating that ml-ILC2s mediate type 2 inflammatory responses in an allergen non-specific manner.

Following infection clearance, effector T cells are acknowledged to undergo a contraction phase, and those survivors (T_{mem}) obtain unique self-renewal property and the ability to recall effector functions upon another specific stimulation[54,55]. BrdU-labeling experiments suggested that ST2$^-$KLRG1$^+$IL-17RB$^+$ ml-ILC2s persisted for a long time, indicating these ml-ILC2s survive from contraction. But the molecular basis of ILC2 contraction is largely unknown. Generally, the exhaustion of T cells is mainly dominated by negative regulatory pathways including cell surface inhibitory receptors like PD-1, soluble cytokines like IL-10, and immunoregulatory T_{reg} cells, etc[56]. Interestingly, KLRG1, expressed on NK cells and antigen-experienced T cells, is also an inhibitory receptor similar to PD-1[57]. Since our data and previous studies[19,20,58] observed that certain subset of ILC2s express KLRG1, it is legitimate that KLRG1 pathway might be responsible for ILC2 contraction. Huang, et al. found that KLRG1^{hi} ILC2s (iILC2s) were inflammatory cells against helminth infection, whereas our data suggested that ST2$^-$KLRG1$^+$IL-17RB$^+$ ml-ILC2s possessed memory and in vivo migrating properties in asthma development. Furthermore, KLRG1 neutralization by antibody blockade in vivo or in vitro followed by adoptive transfer into naive *Rag1*$^{-/-}$ mice prominently inhibit asthmatic changes. These data indicated that KLRG1 neutralization reversed the potency of ml-ILC2s mediating allergic inflammation relapse. Previous study indicates that PD-1 signaling disruption markedly promotes ILC2 in number and the anti-helminth effector function, suggesting PD-1 as an inhibitory factor of ILC2s[36]. Our study showed that mRNA level of *Pdcd1* (encoding PD-1) remained low in both mice and human ST2$^-$KLRG1$^+$IL-17RB$^+$ ILC2s, indicating a different role of PD-1 and KLRG1 in ml-ILC2s development. In addition, IL-17RB might play a role contributing to the high responsiveness of ml-ILC2s. Martinez-Gonzalez et al. speculated that allergen-experienced ST2$^+$Thy1$^+$ILC2s respond more vigorously than naive ILC2s because they expressed high levels of IL-17RB, and IL-25 and IL-33 both can activate them[11]. We found that ST2$^-$KLRG1$^+$IL-17RB$^+$ ml-ILC2s could be induced by IL-25, and the combination of IL-25 and IL-33 further increased ml-ILC2s

https://doi.org/10.1038/s41467-024-52252-2

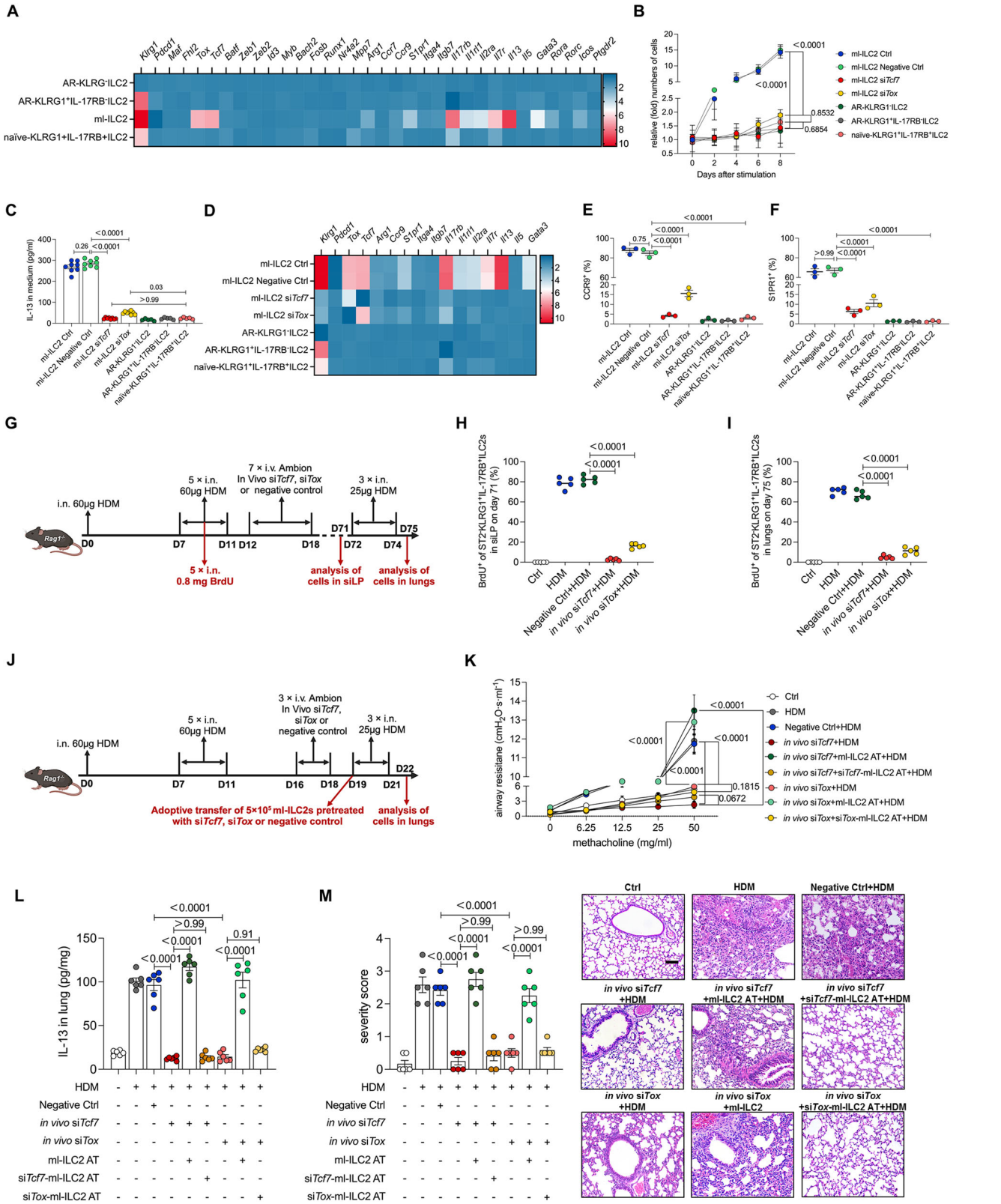

(Fig. S3), similar to ST2⁺Thy1⁺ILC2s in lungs. However, ml-ILC2s are ST2-negative and commonly they cannot be activated by IL-33. The synergistic efficacy of IL-33 might be correlated with its binding with RAGE and EGFR instead of ST2 as reported[24], but in-depth investigation is needed in the future.

Although several studies have implicated ILC2 in memory or trained immunity in context of allergic asthma, the molecular mechanisms underlying remain largely unknown[59]. Constant exposure to *Alternaria* allergen induces transcriptional and epigenetic reprogramming in lung ILC2s. Specifically, the balance between a gene repression program involving *Nr4a2*, *Zeb1*, *Bach2*, and *JunD* and a preparedness program involving *Fhl2*, *FosB*, *Stat6*, *Srebf2*, and *MMP7* contributes to the development of memory ICOS⁺ST2⁺ ILC2s[16]. The transcription factor *Maf* knocked-down ILC2s downregulated several genes involved in T cell memory, indicating an important role of *Maf* in trained immunity of ILC2[47]. In contrast, our data showed that

Fig. 6 | *Tcf7* and *Tox* are essential for memory-like function development of ST2$^-$KLRG1$^+$IL-17RB$^+$ ml-ILC2s. A In asthma remission, KLRG1$^-$, KLRG1$^+$IL-17RB$^-$, KLRG1$^+$IL-17RB$^+$ subsets (marked as AR-KLRG1$^-$, AR-KLRG1$^+$IL-17RB$^-$ and AR-KLRG1$^+$IL-17RB$^+$) in total CD45$^+$lineage$^-$CD90.2$^+$ST2$^-$ ILC2s in siLP were sorted. KLRG1$^+$IL-17RB$^+$ ILC2 (marked as naive-KLRG1$^+$IL-17RB$^+$) were isolated from siLP of naive WT mice ($5 \sim 7 \times 10^5$ for every subset, purity > 98%). Total RNA was isolated, and qRT-PCR was performed. Heat map of mRNA expression values of selected genes (see Fig. S12). $n = 6$ for AR-KLRG1$^-$ILC2, AR-KLRG1$^+$IL-17RB$^-$ ILC2 and AR-KLRG1$^+$IL-17RB$^+$ ILC2, $n = 3$ for naive-KLRG1$^+$IL-17RB$^+$ ILC2. **B**–**F** Sorted CD45$^+$lineage$^-$CD90.2$^+$NK1.1$^-$NKp46$^-$ST2$^-$KLRG1$^+$IL-17RB$^+$ ml-ILC2s were transfected with siRNAs targeting *Tcf7* or *Tox* (si*Tcf7* or si*Tox*) or negative control (Negative Ctrl). Together with AR-KLRG1$^-$, AR-KLRG1$^+$IL-17RB$^-$ and naive-KLRG1$^+$IL-17RB$^+$ ILC2s (5 ± 10^3 per well), a combination of 200 ng/mL IL-25 and 200 ng/mL IL-33 were added every two days with IL-2 and IL-7 for 8 days. Knockdown efficiency of *Tcf7* or *Tox* was confirmed (see Fig. S13A–D). **B** Cell expansion was calculated relative to day 0. **C** Protein levels of IL-13 in culture medium were detected by ELISA. $n = 8$ for ml-ILC2 Ctrl, ml-ILC2 Negative Ctrl, ml-ILC2 si*Tcf7* and ml-ILC2 si*Tox*, $n = 5$ for AR-KLRG1$^-$ILC2, AR-KLRG1$^+$IL-17RB$^-$ ILC2 and naive-KLRG1$^+$IL-17RB$^+$ ILC2. **D** Heat map of mRNA expression values of selected genes (see Fig. S14). $n = 3$. Expression of **E** CCR9 and **F** S1PR1 of all cells in each group were detected with flow cytometry. $n = 3$. **G** Flow chart of asthma mice model, BrdU administration, RNA interference and sample collection. On days 7–11, BrdU (0.8 mg/mice) was given intranasally daily. *Rag1*$^{-/-}$ mice ($n = 5$) were injected with Ambion in vivo si-negative control or indicated siRNAs on days 12–18, and were intranasally treated with 25 μg HDM on days 72-74. The percentage of BrdU$^+$ in ST2$^-$KLRG1$^+$IL-17RB$^+$ILC2s in **H** siLP on day 71 and in (**I**) lungs on day 75 were detected with flow cytometry. **J** Flow chart of asthma mice model, adoptive transfer, RNA interference, and sample collection. *Rag1*$^{-/-}$ mice were exposed with HDM and rested till AHR vanished as described in Fig. S2. Mice were injected with Ambion in vivo si-negative control, si*Tcf7* or si*Tox* on days 16-18, and were intranasally treated with 25 μg HDM on days 19–21. For the groups of in vivo si*Tcf7*+ml-ILC2 AT + HDM and in vivo si*Tox*+ml-ILC2 AT + HDM, mice were injected (i.v.) with 5×10^5 ml-ILC2s precultured with transfection of si-negative control on day 19 before HDM treatment; For the groups of in vivo si*Tcf7*+si*Tcf7*-ml-ILC2 AT + HDM and in vivo si*Tox*+si*Tox*-ml-ILC2 AT + HDM, mice were injected (i.v.) with 5×10^5 ml-ILC2s precultured with transfection of siRNAs on day 19 before HDM treatment. Twenty-four hours after the last HDM treatment, **K** airway resistance ($n = 3$) and **L** IL-13 level in lung homogenates were measured ($n = 6$). **M** Pulmonary histological changes were analyzed ($n = 6$). Magnification: ×200, scale bar = 100 μm. Data was shown as Means ± SD. Results are representative of three independent experiments. Statistical comparison was conducted using unpaired one-way ANOVA with Dunnett's test, except in (**B**) and (**K**) using unpaired two-way ANOVA with the Bonferroni posttest. *p* values are shown on the graphs. Source data are provided as a Source Data file. Fig. 6G, J Created with BioRender.com released under a Creative Commons Attribution-NonCommercial-NoDerivs 4.0 International license https://creativecommons.org/licenses/by-nc-nd/4.0/deed.en.

ST2$^-$KLRG1$^+$IL-17RB$^+$ ml-ILC2s in siLP displayed increased expression of two transcriptional factors *Tcf7* and *Tox*. As a downstream transcriptional factor of Wnt-β-catenin signaling pathway, TCF-1 (encoded by *Tcf7*) is induced by NOTCH signaling and plays a pivotal role in T cell development, differentiation and memory formation[60,61]. Exhausted T cells expressing TCF-1 endowed with self-renewing capability and were indispensable for the long-term maintenance of persistent immune responses[62,63]. Adoptive transfer of TCF-1$^+$ exhausted T cells rapidly repopulated and induced T cell responses in chronic virus infections and tumors, whereas no similar capabilities were found with their TCF-1$^-$ counterparts[62,64]. It is widely held that TOX is a key regulator of T cell exhaustion, but growing evidence suggests this transcription factor is also crucial for T cell memory. Adoptive transfer of retroviral transduction-induced TOX-overexpression significantly enhanced the persistence of lymphocytic choriomeningitis virus (LCMV)-infected CD8$^+$ T cells. Meanwhile, *Tox* deficiency led to a substantial reduction of CD8$^+$ T cells[40]. TOX is also reported as a universal regulator of memory development of CD8$^+$ T cells against chronic virus like cytomegalovirus (CMV), Epstein-Barr virus (EBV) and human immunodeficiency virus (HIV)[41]. Sekine and colleagues[41] also indicated that TOX was expressed primarily in effector memory CD8$^+$ T cells, whereas TCF-1 was expressed primarily in naive and early-differentiated memory CD8$^+$ T cells. In our study, both mice and human memory-like ST2$^-$KLRG1$^+$IL-17RB$^+$ ILC2s in asthma remission express high mRNA levels of *Tcf7* and *Tox*, suggesting both TCF-1 and TOX signaling are required for memory development of ml-ILC2s during asthma relief. Furthermore, expression levels of several genes involved in leukocyte migration including *Ccr9, S1pr1* and *integrin alpha 4 (Itga4)* were elevated in ml-ILC2s comparing to the other two subsets, suggesting a trafficking rather than tissue-resident tendency of ml-ILC2s (Fig. S12B). ST2$^-$KLRG1$^+$IL-17RB$^+$ ml-ILC2s also displayed increased expression of genes associated with ILC2 identity and activation, including *Il1rl1* (encoding the IL-33 receptor), *Il2ra, Il7r, Icos* and *Il13*. In addition, this ILC2 subset expressed high levels of *Gata3* and *Rora*, but no marked difference was identified in the other two subsets (Fig. S12C). Mouse inflammatory ILC2s (iILC2s) are reported to be capable to migrate in vivo and potent to expulse helminth infections[20]. These ILC2s express high levels of KLRG1 and IL-17RB, in line with our ST2$^-$KLRG1$^+$IL-17RB$^+$ ml-ILC2s distinguished in asthma progress. However, mouse iILC2s are also characterized with remarkably decreased levels of intracellular arginase 1 (ARG1), and their activation depend on high expression levels of basic leucine zipper ATF-like transcription factor (BATF)[19,65,66]. In contrast, mRNA levels of *Arg1* and *Batf* of ST2$^-$KLRG1$^+$IL-17RB$^+$ ml-ILC2s in siLP of asthma remission did not show similar variation characteristics (Fig. S12A), suggesting an exclusive role of ml-ILC2s in asthma relapse.

To summarize, we have demonstrated in detail that mice ST2$^-$KLRG1$^+$IL-17RB$^+$ ml-ILC2s generated in airway can migrate to and persistent primarily in distal siLP in asthma remission. Moreover, these ml-ILC2s are endowed with memory-like characteristics including longevity, strong potential of proliferation and expansion and IL-13-producing capability upon allergen or alarmins challenges (Fig. S16). Critically, human CD45$^+$lineage$^-$CRTH2$^+$CD127$^+$GATA3$^+$ST2$^-$KLRG1$^+$IL-17RB$^+$ ILC2s are identical to mice ml-ILC2s in memory-like features and transcriptional hallmarks. Thus, ml-ILC2s mediate a *de facto* innate immune memory, which might be an explanation of why some individuals suffer from severe asthma relapse without being exposed to previously determined allergens. More interestingly, the in vivo trafficking property of ml-ILC2s in different phases of asthma expands our understanding of the gut-lung axis, which has so far focused on microbe-derived components or metabolites like short-chain fatty acids[67]. Our findings on ILC2 memory and migration properties highlight the pivotal role of innate immunological memory during asthma development, and hold great potential for future therapies targeting ml-ILC2s in remission phase instead of restraining inflammatory responses upon asthma attack. However, in-depth investigations need to be applied to investigate the mechanistic roles of TCF and TOX contributing to the memory development of ml-ILC2s in asthma. Besides, more experiments need to be applied to determine whether ml-ILC2s contribute to the relapse of other allergic diseases like rhinitis and whether siLP serves as a shared site for ml-ILC2s to reside.

Methods

Study approval

All animal studies were approved by the Animal Care and Use Committee of Nanjing University of Chinese Medicine, and strictly performed according to the Guide for the Care and Use of Laboratory Animals. All human experimental procedures were reviewed and approved by the Ethical Committee of Nanjing Hospital of Chinese Medicine (KY2019039).

Animals

Mice were maintained under specific pathogen-free conditions with food and water *ad libitum* in the Laboratory Animal Center at Nanjing

https://doi.org/10.1038/s41467-024-52252-2

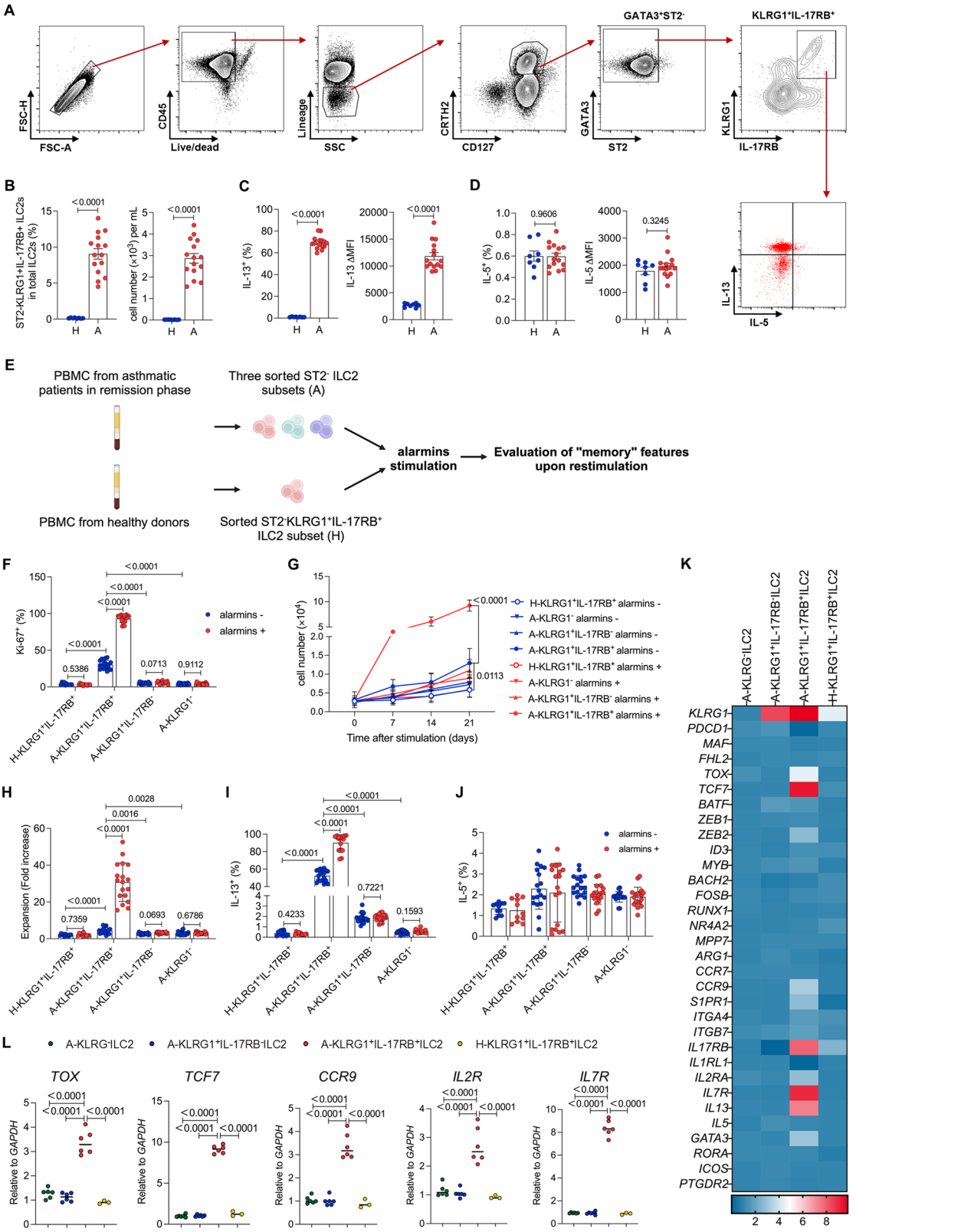

University of Chinese Medicine. The cages were kept at a temperature of 23 ± 3 °C, a humidity of 50 ± 10%, and a 12 h/12 h dark light cycle. C57BL/6 J (WT) mice were purchased from Shanghai SLAC Laboratory Animal Co. Ltd. B6/JGpt-*Rag1*^{em1Cd}/Gpt (*Rag1*$^{-/-}$) mice were purchased from GemPharmatech Co. Ltd (Strain#T004753). B6.SJL-*Ptprc*^{a} *Pepc*^{b}/BoyJ (B6.SJL-CD45.1) mice were purchased from The Jackson Laboratory (Strain#002014). Mice of both sex (6-12 weeks old) were randomly assigned to groups in all experiments.

Human participants

A total of 18 asymptomatic, non-smoking participants with allergic asthma history and 11 healthy volunteers were recruited to the study. Specifically, asthmatic participants were all at remission stage, defined as no wheezing episode for at least more than 50 days. All relevant ethical regulations for work with human donors were complied with, and informed consent was obtained from all participants. See demographics details in Supplementary Data 1.

Fig. 7 | CD45$^+$lineage$^-$CRTH2$^+$CD127$^+$GATA3$^+$ST2$^-$KLRG1$^+$IL-17RB$^+$ ILC2s in peripheral blood of asymptomatic asthmatic patients are identical to mice ml-ILC2s. Flow cytometry was performed to analyze CD45$^+$lineage$^-$CRTH2$^+$CD127$^+$GATA3$^+$ST2$^-$KLRG1$^+$IL-17RB$^+$ ILC2s in PBMCs purified from asthmatic patients during remission phase (all rested for 50 days or longer) and healthy donors. **A** Gating strategy, **B** statistical plots, **C** IL-13$^+$ percentage and MFI and **D** IL-5$^+$ percentage and MFI of CD45$^+$lineage$^-$CRTH2$^+$CD127$^+$GATA3$^+$ST2$^-$KLRG1$^+$IL-17RB$^+$ ILC2s. **E** KLRG1$^-$, KLRG1$^+$IL-17RB$^-$ and KLRG1$^+$IL-17RB$^+$ subsets were purified from the total CD45$^+$lineage$^-$CRTH2$^+$CD127$^+$ST2$^-$ ILC2s in PBMC of 6 asymptomatic asthmatic patients (marked as A-KLRG1$^-$, A-KLRG1$^+$IL-17RB$^-$ and A-KLRG1$^+$IL-17RB$^+$). KLRG1$^+$IL-17RB$^+$ subsets were sorted from total ILC2s in PBMC of 3 healthy donors (marked as H-KLRG1$^+$IL-17RB$^+$). Cells were then cultured (5×10^3/well) with 10 ng/mL IL-2 and 20 ng/mL IL-7, and treated with (alarmins+) or without (alarmins−) 200 ng/mL recombinant human IL-17E/IL-25 and 200 ng/mL recombinant human IL-33 every other day for 21 days. Subsequently, cells were collected for further analysis. **F** Ki-67$^+$ percentage, **G** absolute number and **H** fold changes of expansion of cells were determined. Representative plots and statistical results (bar graph) showing the percentages of **I** IL-13$^+$ and **J** IL-5$^+$ of three ILC2 subsets after stimulation with PMA, ionomycin, brefeldin A and monensin. KLRG1$^-$, KLRG1$^+$IL-17RB$^-$ and KLRG1$^+$IL-17RB$^+$ subsets in total CD45$^+$lineage$^-$CRTH2$^+$CD127$^+$ST2$^-$ ILC2s in PBMC of asymptomatic asthmatic patients (marked as A-KLRG1$^-$, A-KLRG1$^+$IL-17RB$^-$ and A-KLRG1$^+$IL-17RB$^+$) and KLRG1$^+$IL-17RB$^+$ subsets in total ILC2s in PBMC of healthy donors (marked as H-KLRG1$^+$IL-17RB$^+$) were sorted ($4.5 \sim 6.8 \times 10^5$ for every subset, purity > 98%). **K**, **L** Total RNA was isolated, and qRT-PCR was performed. **K** Heat map of mRNA expression values of selected genes. **L** Bar plots of mRNA expression values (relative to *GAPDH*) for genes significantly changed. Data was shown as Means ± SD. $n = 8$ **H** and 15 **A** for (**A**–**D**). $n = 11$ (**H**) and 18 **A** for **E**–**J**. $n = 6$ (A-KLRG1$^-$, A-KLRG1$^+$IL-17RB$^-$ and A-KLRG1$^+$IL-17RB$^+$) and 3 (H-KLRG1$^+$IL-17RB$^+$) for (**K, L**). Statistical comparisons were performed using unpaired, two-sided Welch's *t* test for (**B**–**D**), and unpaired one-way ANOVA with Dunnett's test for (**L**). *p* values are shown on the graphs. Source data are provided as a Source Data file. Fig. 7E Created with BioRender.com released under a Creative Commons Attribution-NonCommercial-NoDerivs 4.0 International license https://creativecommons.org/licenses/by-nc-nd/4.0/deed.en.

HDM sensitization and challenges

A 24-day HDM-induced asthma model (hereinafter referred as the i.p. HDM sensitization model) was established as described previously[68]. Briefly, mice were given intraperitoneal injection (i.p.) of 50 μg HDM (#B82; Stallergenes Greer) for three times on days 0, 7, and 14, followed by 3 consecutive intranasal challenges (i.n.) of 25 μg HDM to elicit asthmatic responses on days 21–23. To elicit asthma recurrence, model mice rested from AHR were re-exposed to 25 μg HDM on days 31-33. For another 12-day asthma model (hereinafter referred as the i.n. HDM sensitization model)[69], mice were sensitized with 60 μg HDM (i.n.) on day 0, followed by 5-time challenges with 60 μg HDM (i.n.) on days 7–11. Mice were euthanized by overdose of isoflurane and samples were collected at indicated time points. To collect BALF, the trachea was exposed and cannulated with 20 G catheter. 0.8 mL 1× PBS at 4 °C was gently infused followed by extraction, and this procedure was repeated 3 times. Total recovered volume was ~2.5–2.7 mL/mouse. In the experiments with cytokine quantification and histology observation, left lung lobes were ligated, and only right lung lobes were infused with 0.5 mL 1× pre-cold PBS for 3 times. The BALF was then centrifuged at 1500RPM for 10 minutes at 4 °C. The supernatant was discarded, and remaining cell pellets were resuspended with 1 mL 1× PBS (4 °C). Total cells counting was performed on Countstar (Alit Biotech). For cytology investigation, cells were stained with Wright-Giemsa Staining Solution (#C0131-500mL; Beyotime), and eosinophils, neutrophils, macrophages and lymphocytes were enumerated and analyzed with hemocytometers.

Measurement of airway responsiveness

Under anesthesia by isoflurane, airway resistance of mice was measured post trachea intubation under the exposure of increasing doses of aerosolized methacholine (#1396364; Sigma-Aldrich) at 0, 6.25, 12.5, 25, 50 mg/mL diluted in PBS. Data was collected from Buxco Pulmonary Function Test (DSI). Before administration of the next doses of methacholine, resistance was ensured to return to baseline. Airway resistance under each dose of methacholine was calculated using 20 measurements.

Preparation of cell suspensions

Human and mice PBMCs were enriched from peripheral blood by a Percoll (#FMS-FL01; FCMACS) gradient centrifugation at 800 × *g* for 20 min. LNs were harvested and single-cell suspensions were obtained through 70 μm-cell strainers. SI were opened longitudinally, and washed twice with ice cold PBS for removing the contents. Peyer's patches were removed and tissues were mechanically disrupted into small pieces, and then incubated at 37 °C for 50 min in PBS containing 5 mM EDTA to dissociate intraepithelial leukocytes. The remained fragments were washed twice with ice-cold PBS and then incubated at for 55 min with Liberase TM (200 μg/mL) (#5401127001; Sigma-Aldrich) plus DNase I (10 μg/mL) (#10104159001; Sigma-Aldrich). For isolation of cells from lungs and trachea, tissues were disrupted by scissors, then were digested for 35 min at 37 °C in an enzyme mix composed of Liberase TM plus DNase I. Single-cell suspension was then yielded by straining digested tissues, followed by ACK solution (#FMS-RBC100; FCMACS) treatment. Leukocytes were washed and further enriched by a Percoll gradient centrifugation before further analysis.

Flow cytometry and cell sorting

To analyze mice ILC2s, different combinations of antibodies against lineage markers (CD3ε, clone 145-2C11, Ly-6G/Ly-6C, clone RB6-8C5, CD11b, clone M1/70, CD45R/B220, clone RA3-6B2, TER-119/Erythroid cells, clone Ter-119; #133302; BioLegend; 1:200), CD45 (clone 30-F11; #25-0451-82; eBioscience; 1:500), CD90.2/Thy1.2 (clone 53-2.1; #64-0902-82; eBioscience; 1:500), NK1.1 (clone PK136; #414-5941-82; eBioscience; 1:500), NKp46/CD335 (clone 29A1.4; #48-3351-82; eBioscience; 1:500), CD4 (clone RM4-5; #Q22165; eBioscience; 1:500), IL-33R/ST2 (clone RMST2-2; #63-9335-82; eBioscience; 1:200), GATA3 (clone TWAJ; #56-9966-42; eBioscience; 1:100), Rorγt (clone B2D; #61-6981-82; eBioscience; 1:100), KLRG1 (clone 2F1; #46-5893-80; eBioscience; 1:200), IL-17RB (clone MUNC33; #50-7361-82; eBioscience; 1:200), CD199/CCR9 (clone CW-1.2; #48-1991-82; eBioscience; 1:500), CD363/S1PR1 (clone SW4GYPP; #50-3639-42; eBioscience; 1:500), integrin α4β7 (clone DATK-32; #12-5887-82; eBioscience; 1:500), CD45.1 (clone A20; #48-0453-82; eBioscience; 1:500), Ki-67 (clone SolA15; #46-5698-82; eBioscience; 1:500), IL-4 (clone 11B11; # 25-7041-82; eBioscience; 1:200), IL-5 (clone TRFK5; #12-7052-81; eBioscience; 1:200), IL-13 (clone eBio13A; #47-7133-80; eBioscience; 1:200), TCF-1 (clone C.725.7; #MA5-14965; invitrogen; 1:200) and TOX (clone TXRX10; #12-6502-82; Invitrogen; 1:200) or corresponding control isotypes were applied depending on the experiment. Cells were blocked with FcR Blocking Reagent (#130-092-575, Miltenyi Biotec), followed by 30 min of staining with antibodies and with LIVE/DEAD Fixable aqua at 4 °C. Total mice ILC2s are identified as live CD45$^+$lineage$^-$CD90.2$^+$NK1.1$^-$NKp46$^-$GATA3$^+$, and memory-like ILC2s (ml-ILC2s) are gated as CD45$^+$lineage$^-$CD90.2$^+$NK1.1$^-$NKp46$^-$GATA3$^+$ST2$^-$KLRG1$^+$IL-17RB$^+$. For intracellular analysis, cells were treated with 1× Cell Stimulation Cocktail (plus protein transport inhibitors) (#00-4975-93; eBioscience) and the Foxp3/Transcription Factor Staining Buffer Set (#00-5523-00; eBioscience) according to the manufacturer's instructions before antibody staining. To analyze human ILC2s, antibodies against CD45 (clone HI30; #MHCD4512; Invitrogen; 1:500), lineage markers (CD2, clone RPA-2.10, CD3, clone OKT3, CD14, clone 61D3, CD16, clone CB16, CD19, clone HIB19, CD56, clone TULY56, and CD235a, clone HIR2; #22-7778-72; eBioscience; 1:250), CRTH2 (clone BM16; #12-2949-41; eBioscience;

1:500), CD127 (clone eBioRDR5; #15-1278-42; Invitrogen; 1:500), GATA3 (clone TWAJ; #48-9966-42; Invitrogen; 1:200), ST2 (clone hIL33Rcap; #46-9338-42; Invitrogen; 1:200), KLRG1 (clone 47-9488-41; #47-9488-41; eBioscience; 1:200), IL-17RB (clone 170220; #FAB1207A; R&D systems; 1:200), IL-13 (clone 85BRD; #51-7136-42; Invitrogen; 1:200), IL-5 (clone TRFK5; #48-7052-82; Invitrogen; 1:200), Ki-67 (clone SolA15; #53-5698-82; Invitrogen; 1:500) and corresponding isotype controls were applied. Samples were prepared as described in mice ILC2 analysis. Total human ILC2s are defined as live $CD45^+lineage^-CRTH2^+CD127^+GATA3^+$, and human memory-like ILC2s are $CD45^+lineage^-CRTH2^+CD127^+GATA3^+ST2^-KLRG1^+IL\text{-}17RB^+$ ILC2s. Cells were acquired on Cytoflex S (Beckman Coulter) and analyzed with FlowJo v10.4 software (TreeStar).

Lineage-negative cells from mice bone marrow, spleen, lungs and siLP were enriched with Lineage Cell Depletion kit (#130-090-858; Miltenyi Biotec) according to the manufacturer's instructions. To sort ml-ILC2s and other ILC2 subsets, lineage-negative cells of asthmatic mice in remission phase were magnetically enriched, and purified by fluorescence-activated cell sorting on FACS Aria III cell sorter (BD Bioscience).

In vitro cell culture

Mice $CD45^+$Lineage-negative cells ($3–5 \times 10^5$) were cultured in round-bottom plates with irradiated PBMCs (25 Gy, 1×10^6/mL) in complete RPMI medium containing 10% FBS, 10 ng/mL IL-2 (#212-12; peprotech) and 20 ng/mL IL-7 (#217-17; peprotech) for 30 days. For the source confirmation of lung ml-ILC2s upon HDM recall, $lineage^-CD90.2^+NK1.1^-NKp46^-ST2^-KLRG1^+IL\text{-}17RB^+$ were re-sorted after expansion. For the proliferation, expansion and cytokine production analysis, $KLRG1^+IL\text{-}17RB^+$, $KLRG1^+IL\text{-}17RB^-$ and $KLRG1^-$ subsets from total $CD45^+lineage^-CD90.2^+NK1.1^-NKp46^-ST2^-$ cells in siLP were purified and seeded in round-bottom culture wells (5×10^3/well). Combination of alarmins including 200 ng/mL IL-25 (#7909-IL-010/CF; R&D Systems) and 200 ng/mL IL-33 (#3626-ML-010/CF; R&D Systems) were added every two days with IL-2 and IL-7 for 14 days before flow cytometry analysis.

For the KLRG1 neutralization and adoptive experiment, $CD45^+lineage^-CD90.2^+NK1.1^-NKp46^-ST2^-KLRG1^+IL\text{-}17RB^+$ ml-ILC2s were sorted from siLP of *Rag1*$^{-/-}$ mice in asthma remission, and expanded with 10 ng/mL IL-2 and 20 ng/mL IL-7. The culture was incubated with 0.75 μg/mL anti-KLRG-1 (clone 2F1, #BE0201; BioXCell) or isotype IgG (#BE0087; BioXCell) for 3 consecutive days before adoptive transfer.

Sort-purified human $CD45^+lineage^-CRTH2^+CD127^+$ILC2s were expanded for 5 weeks with irradiated PBMCs (Co60, 25 Gy, 2×10^6/mL) in RPMI medium with 10% heat-inactivated FBS, 2 mM glutamine, 100 IU/mL recombinant IL-2 and 100 IU/mL recombinant IL-7 (Cat#200-02 and Cat#200-07; Peprotech) in Ultra-Low Attachment flasks (Corning). Afterwards, $CD45^+lineage^-CRTH2^+CD127^+ST2^-KLRG1^+IL\text{-}17RB^+$, $CD45^+lineage^-CRTH2^+CD127^+ST2^-KLRG1^+IL\text{-}17RB^-$ and $CD45^+lineage^-CRTH2^+CD127^+ST2^-KLRG1^-$ subsets from culture cells were re-sorted, and then seeded in 96-well round-bottom plates at the density of 5×10^3 cells per well. A combination of 200 ng/mL IL-17E/IL-25 (Cat#200-24; Peprotech) and 200 ng/mL IL-33 (#3625-IL-010/CF; R&D Systems) were added every two days with IL-2 and IL-7 for 21 days, followed by flow cytometry analysis.

RNA interference

In vitro, 6 pmol Silencer Select si*Tcf7*, si*Tox* (#4390771; invitrogen) or Silencer Select Negative Control #1 siRNA (#4390843; invitrogen) in 100 μL of Opti-MEM was mixed with 1 μL Lipofectamine RNAiMAX (#13778150; invitrogen), and incubated for 20 min at room temperature. Cultured ml-ILC2s (5×10^3 in 500 μL RPMI medium per well) were added in. Combination of 200 ng/mL IL-17E/IL-25 (Cat#200-24; Peprotech) and 200 ng/mL IL-33 (#3625-IL-010/CF; R&D Systems) were added every 2 days with IL-2 and IL-7 for 8 days before further analysis. For In vivo studies, 100 μL of Ambion In Vivo si*Tcf7*, si*Tox* (#4457308; invitrogen) or Ambion In Vivo Negative Control #1 siRNA (#4457287; invitrogen) solution (1.2 mg/mL) was mixed with 100 μL of Invivofectamine 3.0 Reagent (#IVF3001; invitrogen), and incubated for 30 min at 50 °C. Dilute the complex by adding 1 mL of PBS, and injected into *Rag1*$^{-/-}$ mice in asthma remission (day 19 of the airway stimulation model) via tail vein (10 μL/g body weight). Mice were then intranasally exposed to 25 μg HDM once per day on days 19-21. Asthmatic responses were evaluated 24 hours after the last HDM stimulation.

Neutralization of KLRG1

For in vivo KLRG1 neutralization, WT or *Rag1*$^{-/-}$ mice were injected with 10 mg/kg *InVivo*MAb anti-mouse KLRG-1 (clone 2F1, #BE0201; BioXCell) or isotype IgG (#BE0087; BioXCell) intraperitoneally on day 0, 7, 14 and 21 of the i.p. HDM sensitization model. For adoptive transfer experiments, $CD45^+lineage^-CD90.2^+NK1.1^-NKp46^-ST2^-KLRG1^+IL\text{-}17RB^+$ ml-ILC2s purified from siLP of asthmatic *Rag1*$^{-/-}$ mice were expanded in vitro, followed by incubation with anti-KLRG-1 or isotype IgG. Afterwards, cells were injected into T/B/ILC-deficient mice via tail vein for further analysis.

Adoptive transfer

Sorted $CD45^+lineage^-CD90.2^+NK1.1^-NKp46^-ST2^-KLRG1^+IL\text{-}17RB^+$ ml-ILC2s of expanded lineage-negative cells from bone marrow, spleen, lungs or siLP of asthmatic $CD45.1^+$ mice during mission phase were injected into irradiated $CD45.2^+$ mice (5×10^5 donor cells per mouse) via tail vein. In the KLRG1 neutralization/adoptive transfer experiment, naive *Rag1*$^{-/-}$ mice were treated with 200 μg *InVivo*Plus anti-mouse Thy1.2 (CD90.2) (clone30H12, #BP0066; BioXCell) to deplete ILCs or isotype IgG2b (#BE0090; BioXCell) intraperitoneally on day 1, 3 and 5 prior to the injection (i.v.) of 5×10^5 ml-ILC2s with/without pretreatment of siRNAs on indicated days. Afterwards, 25 μg HDM or 500 ng recombinant IL-25 (#7909-IL-025; R&D Systems) was intranasally administered to recipient mice every 24 hours for 3 consecutive days, followed by further analysis 24 hours after last administration.

Parabiosis

$CD45.2^+$ WT mice were sublethally irradiated (Co60, 10 Gy) and parabiosed to $CD45.1^+$ mice of similar size as described previously[70]. Briefly, each pair of mice cohabitated harmoniously were anesthesized, and surgical areas on the opposite sides of two mice were thoroughly shaved and further asepticized with betadine and alcohol. Incisions were made in the skin, and the elbow joints and knee joints of two mice were anchored, followed by skin connection and sterile saline administration to prevent dehydration. Mice were then intramuscularly administered with dezocine every 12 hours for 3 days to provide analgesics. Water containing 10^6 U/liter polymyxin B sulfate and 1.1 g/L neomycin sulfate were provided to parabiotic mice for 2 weeks post-surgery. Establishment of HDM-induced asthma model was performed on $CD45.1^+$ mice 4 weeks after surgery.

Bromodeoxyuridine (BrdU) labeling

On days 21 to 23 of the i.p. HDM sensitization model and days 7 to 11 of the i.n. HDM sensitization model, mice were intranasally administered with 0.8 mg BrdU (#559619; BD Biosciences) dissolved in 30 μL PBS. On days 1, 30, 60, and 90 (i.p. HDM sensitization model) and 7 and 60 (i.n. HDM sensitization model) after the last intranasal exposure of HDM, single-cell suspensions were prepared from siLP prior to flow cytometry analysis.

Xenolight DiR imaging

Sorted 5×10^5 mice ml-ILC2s from siLP in 940 μL PBS were stained with 60 μL of Xenolight DiR (#125964; PerkinElmer) at 5 mM. After incubation at 37 °C for 30 min, cell pellet was washed twice and resuspended in PBS before adoptive transfer into mice at the stage of

asthma attack or remission. For the mice in the remission + CCX282-B group, HDM-induced asthmatic mice were treated with the selective antagonist of CCR9 CCX282-B (50 mg/kg, injected subcutaneously) (#698394-73-9; Axon Medchem) or vehicle daily from day 24 to day 30, followed by ml-ILC2s transfer. Mice in the remission + Etrolizumab group were treated with the anti-α4β7 monoclonal antibody Etrolizumab (injected via tail vein, 5 mg/kg) (#1044758-60-2; MedChemExpress) on days 24, 26, 28, and 30. And for the relapse groups, mice during remission phase of asthma received ml-ILC2s transfer, and were injected intravenously with FTY720 (1 mg/kg) (#HY-12005; MedChemExpress) or vehicle for 2 times along with the intranasal administration of HDM (50 μg) once per hour concurrently. Two hours after ml-ILC2s injection, mice in all groups were imaged ventrally with IVIS optical imaging systems (PerkinElmer), and organs including lungs, spleen, liver, SI and large intestine were then rapidly harvested for ex vivo imaging. Filter set was 710 nm excitation and 760 nm emission, and images were acquired under the same scale setting.

Enzyme-linked immunosorbent assays (ELISA)

Mouse IL-4, IL-5, IL-13, IL-17A, IgE, CCL25, MAdCAM-1 and S1P concentrations in indicated samples were detected by performing ELISA assays according to the manufacturers' instructions (mouse IL-4, IL-5, IL-13, IL-17A and IgE: #88-7044-86, #88-7054-86, #88-7137-88, # 88-7371-86 and #88-50460-88; Invitrogen, mouse CCL25 and MAdCAM-1: #DY481 and #DY2768; R&D systems and mouse S1P: #K-1900, Echelon). Mouse IL-4, IL-5, IL-13 in lungs, and CCL25 and MAdCAM-1 in SI homogenates were adjusted by the total protein level detected by BCA protein assays.

Quantitative real-time reverse transcriptase PCR (qRT-PCR)

RNA was isolated from sorted mice or human ILC2s ($5 \sim 7 \times 10^5$) using the RNeasy Micro Kit (#74004; Qiagen) according to the manufacturer's instructions. RNA was synthesized into complementary DNA with HiScript II 1st Strand cDNA Synthesis Kit (R211-01; Vazyme Biotech) in the presence of RiboLock RNase inhibitor (#EO0381, Thermo Fisher Scientific). qRT-PCR was performed with SYBR Green PCR Master Mix were used (#Q511-02; Vazyme Biotech) using ABI 7500 Fast Real-Time PCR platform (Applied Biosystems). Quantification of relative gene expression was analyzed using $2^{-\Delta\Delta Ct}$, and normalized to *Gapdh/GAPDH*. Primers used are listed in Supplementary Data 2.

Histology

Tissues were fixed in 4% paraformaldehyde and embedded in paraffin. Sections at 6 μm were dewaxed and hydrated before hematoxylin and eosin staining. Images were acquired by the Mantra system (PerkinElmer). Lung slices were scored for severity of airway inflammation by a histopathologist in a blinded manner according to the following scoring system: 0, normal; 0.5, very mild; 1, mild; 1.5, mild-moderate; 2, moderate; 2.5, moderate-severe; 3, severe.

Statistics

No data were excluded from analysis. Statistical analysis was performed with GraphPad Prism software version 9.5.0 (GraphPad). Data are shown as mean ± SD. A p value ≤ 0.05 was considered statistically significant. Unpaired, two-sided Welch's t-test, unpaired one-way analysis of variance (ANOVA) with Dunnett's test or unpaired two-way ANOVA with the Bonferroni posttest were used as indicated.

Reporting summary

Further information on research design is available in the Nature Portfolio Reporting Summary linked to this article.

Data availability

This study does not include data deposited in external repositories. All other data are available in the article and its Supplementary files or from the corresponding author upon request. Source data are provided with this paper.

References

1. Collaborators, G. B. D. C. R. D. Global, regional, and national deaths, prevalence, disability-adjusted life years, and years lived with disability for chronic obstructive pulmonary disease and asthma, 1990-2015: a systematic analysis for the Global Burden of Disease Study 2015. *Lancet Respir. Med.* **5**, 691–706 (2017).
2. Huang, K. et al. Prevalence, risk factors, and management of asthma in China: a national cross-sectional study. *Lancet* **394**, 407–418 (2019).
3. To, T. et al. Global asthma prevalence in adults: findings from the cross-sectional world health survey. *BMC Public Health* **12**, 204 (2012).
4. Huang, G. et al. Microwave-assisted, rapid synthesis of 2-vinylquinolines and evaluation of their antimalarial activity. *Tetrahedron Lett.* **60**, 1736–1740 (2019).
5. Balbino, B. et al. The anti-IgE mAb omalizumab induces adverse reactions by engaging Fcgamma receptors. *J. Clin. Invest.* **130**, 1330–1335 (2020).
6. Di Salvo, E., Patella, V., Casciaro, M. & Gangemi, S. The leukotriene receptor antagonist montelukast can induce adverse skin reactions in asthmatic patients. *Pulm. Pharm. Ther.* **60**, 101875 (2020).
7. Zhang, Y. et al. The safety and efficacy of anti-IL-13 treatment with tralokinumab (CAT-354) in moderate to severe asthma: a systematic review and meta-analysis. *J. Allergy Clin. Immunol. Pract.* **7**, 2661–2671.e2663 (2019).
8. Hammad, H. & Lambrecht, B. N. The basic immunology of asthma. *Cell* **184**, 1469–1485 (2021).
9. Moro, K. et al. Innate production of T(H)2 cytokines by adipose tissue-associated c-Kit(+)Sca-1(+) lymphoid cells. *Nature* **463**, 540–544 (2010).
10. Wallrapp, A., Riesenfeld, S. J., Burkett, P. R. & Kuchroo, V. K. Type 2 innate lymphoid cells in the induction and resolution of tissue inflammation. *Immunol. Rev.* **286**, 53–73 (2018).
11. Martinez-Gonzalez, I. et al. 2 memory: Recollection of previous activation. *Immunol. Rev.* **283**, 41–53 (2018).
12. Sun, J. C., Beilke, J. N. & Lanier, L. L. Adaptive immune features of natural killer cells. *Nature* **457**, 557–561 (2009).
13. Nabekura, T. & Lanier, L. L. Tracking the fate of antigen-specific versus cytokine-activated natural killer cells after cytomegalovirus infection. *J. Exp. Med* **213**, 2745–2758 (2016).
14. Martinez-Gonzalez, I. et al. Allergen-experienced group 2 innate lymphoid cells acquire memory-like properties and enhance allergic lung inflammation. *Immunity* **45**, 198–208 (2016).
15. Seehus, C. R. et al. Alternative activation generates IL-10 producing type 2 innate lymphoid cells. *Nat. Commun.* **8**, 1900 (2017).
16. Verma M. et al. The molecular and epigenetic mechanisms of innate lymphoid cell (ILC) memory and its relevance for asthma. *J Exp. Med.* **218**, e20201354 (2021).
17. Joshi, N. S. et al. Inflammation directs memory precursor and short-lived effector CD8(+) T cell fates via the graded expression of T-bet transcription factor. *Immunity* **27**, 281–295 (2007).
18. Nagasawa, M. et al. KLRG1 and NKp46 discriminate subpopulations of human CD117(+)CRTH2(-) ILCs biased toward ILC2 or ILC3. *J. Exp. Med* **216**, 1762–1776 (2019).
19. Huang, Y. et al. IL-25-responsive, lineage-negative KLRG1(hi) cells are multipotential 'inflammatory' type 2 innate lymphoid cells. *Nat. Immunol.* **16**, 161–169 (2015).
20. Huang, Y. et al. S1P-dependent interorgan trafficking of group 2 innate lymphoid cells supports host defense. *Science* **359**, 114–119 (2018).
21. Salimi, M. et al. A role for IL-25 and IL-33-driven type-2 innate lymphoid cells in atopic dermatitis. *J. Exp. Med.* **210**, 2939–2950 (2013).

22. Ricardo-Gonzalez R. R. et al. Tissue-specific pathways extrude activated ILC2s to disseminate type 2 immunity. *J. Exp. Med*. **217**, 2202210 (2020).
23. Xu, H. et al. Transcriptional atlas of intestinal immune cells reveals that neuropeptide alpha-CGRP modulates group 2 innate lymphoid cell responses. *Immunity* **51**, 696–708 e699 (2019).
24. Strickson S. et al. Oxidised IL-33 drives COPD epithelial pathogenesis via ST2-independent RAGE/EGFR signalling complex. *Eur. Respir. J.* **62**, 2202210 (2023).
25. Akdis, M. et al. Interleukins (from IL-1 to IL-38), interferons, transforming growth factor beta, and TNF-alpha: Receptors, functions, and roles in diseases. *J. Allergy Clin. Immunol*. **138**, 984–1010 (2016).
26. Wu, L. C. & Zarrin, A. A. The production and regulation of IgE by the immune system. *Nat. Rev. Immunol*. **14**, 247–259 (2014).
27. Kim, M. H., Taparowsky, E. J. & Kim, C. H. Retinoic acid differentially regulates the migration of innate lymphoid cell subsets to the gut. *Immunity* **43**, 107–119 (2015).
28. Bouskra, D. et al. Lymphoid tissue genesis induced by commensals through NOD1 regulates intestinal homeostasis. *Nature* **456**, 507–510 (2008).
29. Klose, C. S. et al. A T-bet gradient controls the fate and function of CCR6-RORgammat+ innate lymphoid cells. *Nature* **494**, 261–265 (2013).
30. Possot, C. et al. Notch signaling is necessary for adult, but not fetal, development of RORgammat(+) innate lymphoid cells. *Nat. Immunol*. **12**, 949–958 (2011).
31. Kadowaki, A., Saga, R., Lin, Y., Sato, W. & Yamamura, T. Gut microbiota-dependent CCR9+CD4+ T cells are altered in secondary progressive multiple sclerosis. *Brain* **142**, 916–931 (2019).
32. Zhu, Z. et al. IL-13-induced chemokine responses in the lung: role of CCR2 in the pathogenesis of IL-13-induced inflammation and remodeling. *J. Immunol*. **168**, 2953–2962 (2002).
33. Youngblood, B. et al. Effector CD8 T cells dedifferentiate into long-lived memory cells. *Nature* **552**, 404–409 (2017).
34. Fife, B. T. et al. Interactions between PD-1 and PD-L1 promote tolerance by blocking the TCR-induced stop signal. *Nat. Immunol*. **10**, 1185–1192 (2009).
35. Helou, D. G. et al. PD-1 pathway regulates ILC2 metabolism and PD-1 agonist treatment ameliorates airway hyperreactivity. *Nat. Commun*. **11**, 3998 (2020).
36. Taylor, S. et al. PD-1 regulates KLRG1(+) group 2 innate lymphoid cells. *J. Exp. Med* **214**, 1663–1678 (2017).
37. Kallies, A., Zehn, D. & Utzschneider, D. T. Precursor exhausted T cells: key to successful immunotherapy? *Nat. Rev. Immunol*. **20**, 128–136 (2020).
38. Giles, J. R. et al. Shared and distinct biological circuits in effector, memory and exhausted CD8(+) T cells revealed by temporal single-cell transcriptomics and epigenetics. *Nat. Immunol*. **23**, 1600–1613 (2022).
39. O'Flaherty, E. & Kaye, J. TOX defines a conserved subfamily of HMG-box proteins. *BMC Genomics* **4**, 13 (2003).
40. Yao, C. et al. Single-cell RNA-seq reveals TOX as a key regulator of CD8(+) T cell persistence in chronic infection. *Nat. Immunol*. **20**, 890–901 (2019).
41. Sekine T. et al. TOX is expressed by exhausted and polyfunctional human effector memory CD8(+) T cells. *Sci. Immunol*. **5**, eaba7918 (2020).
42. Yao, C. et al. BACH2 enforces the transcriptional and epigenetic programs of stem-like CD8(+) T cells. *Nat. Immunol*. **22**, 370–380 (2021).
43. Gautam, S. et al. The transcription factor c-Myb regulates CD8(+) T cell stemness and antitumor immunity. *Nat. Immunol*. **20**, 337–349 (2019).
44. Roychoudhuri, R. et al. BACH2 regulates CD8(+) T cell differentiation by controlling access of AP-1 factors to enhancers. *Nat. Immunol*. **17**, 851–860 (2016).
45. Yang, C. Y. et al. The transcriptional regulators Id2 and Id3 control the formation of distinct memory CD8+ T cell subsets. *Nat. Immunol*. **12**, 1221–1229 (2011).
46. Gonzalez, N. M., Zou, D., Gu, A. & Chen, W. Schrodinger's T cells: molecular insights into stemness and exhaustion. *Front Immunol*. **12**, 725618 (2021).
47. Trabanelli, S. et al. c-Maf enforces cytokine production and promotes memory-like responses in mouse and human type 2 innate lymphoid cells. *EMBO J*. **41**, e109300 (2022).
48. O'Sullivan, T. E., Sun, J. C. & Lanier, L. L. Natural killer cell memory. *Immunity* **43**, 634–645 (2015).
49. Sallusto, F., Lenig, D., Forster, R., Lipp, M. & Lanzavecchia, A. Two subsets of memory T lymphocytes with distinct homing potentials and effector functions. *Nature* **401**, 708–712 (1999).
50. Gasteiger, G., Fan, X., Dikiy, S., Lee, S. Y. & Rudensky, A. Y. Tissue residency of innate lymphoid cells in lymphoid and nonlymphoid organs. *Science* **350**, 981–985 (2015).
51. Moro, K. et al. Interferon and IL-27 antagonize the function of group 2 innate lymphoid cells and type 2 innate immune responses. *Nat. Immunol*. **17**, 76–86 (2016).
52. Halim, T. Y., Krauss, R. H., Sun, A. C. & Takei, F. Lung natural helper cells are a critical source of Th2 cell-type cytokines in protease allergen-induced airway inflammation. *Immunity* **36**, 451–463 (2012).
53. Halim, T. Y. et al. Group 2 innate lymphoid cells are critical for the initiation of adaptive T helper 2 cell-mediated allergic lung inflammation. *Immunity* **40**, 425–435 (2014).
54. Ataide, M. A. et al. BATF3 programs CD8(+) T cell memory. *Nat. Immunol*. **21**, 1397–1407 (2020).
55. Kumar, B. V., Connors, T. J. & Farber, D. L. Human T cell development, localization, and function throughout life. *Immunity* **48**, 202–213 (2018).
56. Wherry, E. J. T cell exhaustion. *Nat. Immunol*. **12**, 492–499 (2011).
57. Henson, S. M. & Akbar, A. N. KLRG1-more than a marker for T cell senescence. *Age (Dordr.)* **31**, 285–291 (2009).
58. Hoyler, T. et al. The transcription factor GATA-3 controls cell fate and maintenance of type 2 innate lymphoid cells. *Immunity* **37**, 634–648 (2012).
59. Hartung, F. & Esser-von Bieren, J. Trained immunity in type 2 immune responses. *Mucosal Immunol*. **15**, 1158–1169 (2022).
60. Zhang, J., Lyu, T., Cao, Y. & Feng, H. Role of TCF-1 in differentiation, exhaustion, and memory of CD8(+) T cells: a review. *FASEB J*. **35**, e21549 (2021).
61. Wen, S. et al. TCF-1 maintains CD8(+) T cell stemness in tumor microenvironment. *J. Leukoc. Biol*. **110**, 585–590 (2021).
62. Utzschneider, D. T. et al. T Cell Factor 1-expressing Memory-like CD8(+) T Cells Sustain The Immune Response To Chronic Viral Infections. *Immunity* **45**, 415–427 (2016).
63. Im, S. J. et al. Defining CD8+ T cells that provide the proliferative burst after PD-1 therapy. *Nature* **537**, 417–421 (2016).
64. Miller, B. C. et al. Subsets of exhausted CD8(+) T cells differentially mediate tumor control and respond to checkpoint blockade. *Nat. Immunol*. **20**, 326–336 (2019).
65. Miller M. M. et al. BATF acts as an essential regulator of IL-25-responsive migratory ILC2 cell fate and function. *Sci. Immunol*. **5**, eaay3994 (2020).
66. Flamar, A. L. et al. Interleukin-33 Induces The Enzyme Tryptophan Hydroxylase 1 To Promote Inflammatory Group 2 Innate Lymphoid Cell-mediated Immunity. *Immunity* **52**, 606–619.e606 (2020).
67. Dang, A. T. & Marsland, B. J. Microbes, metabolites, and the gut-lung axis. *Mucosal Immunol*. **12**, 843–850 (2019).

68. Bao, K. et al. A chinese prescription Yu-Ping-Feng-San administered in remission restores bronchial epithelial barrier to inhibit house dust mite-induced asthma recurrence. *Front Pharm.* **10**, 1698 (2019).
69. Everaere, L. et al. Innate lymphoid cells contribute to allergic airway disease exacerbation by obesity. *J. Allergy Clin. Immunol.* **138**, 1309–1318 e1311 (2016).
70. Kamran, P. et al. Parabiosis in mice: a detailed protocol. *J. Vis. Exp.* **6**, 50556 (2013).

Acknowledgements

We express our gratitude to Professor Yang Sun (Nanjing University) for his kind assistance, advice, and discussions throughout this study. We thank Yunxian Sun and Guang Wang (Nanjing University of Aeronautics and Astronautics) for help with γ-ray irradiation. This work is supported by the National Natural Science Foundation of China (grants 82074087, 82204714, and 81703733), Natural Science Foundation of Jiangsu Province (grant BK20191414), Key project of Jiangsu Administration of Traditional Chinese Medicine (grant ZD201902), Key Natural Science Project of Jiangsu Education Department (grant 20KJA360005) and Supporting Funds for the Youth Program of the National Natural Science Foundation of Nanjing University of Chinese Medicine (grant XPT82204714).

Author contributions

K.F.B. and M.H. conceptualized the study; K.F.B., X.Q.G., Y.J.S., Y.J.Z., Y.Y.C., L.Y.S., J.Z., and M.H. devised the methodology; K.F.B., X.Q.G., Y.J.S., Y.J.Z., Y.Y.C, X.Y., W.Y.Y., and J.Z. carried out the investigation; K.F.B., M.H., X.Y., and L.Y.S. wrote the manuscript; M.H. supervised the study.

Competing interests

The authors declare no competing interests.

Additional information

Supplementary information The online version contains supplementary material available at https://doi.org/10.1038/s41467-024-52252-2.

Correspondence and requests for materials should be addressed to Kaifan Bao, Jie Zheng or Min Hong.

Peer review information *Nature Communications* thanks Hye Young Kim, Simon Phipps and the other, anonymous, reviewer(s) for their contribution to the peer review of this work. A peer review file is available.